A geophysical study of a drumlin in the Åsnen area, Småland, south Sweden

Besnik Asani

Dissertations in Geology at Lund University,
Bachelor's thesis, no 444
(15 hp/ECTS credits)

Department of Geology
Lund University
2015

A geophysical study of a drumlin in the Åsnen area, Småland, south Sweden

Bachelor's thesis

Besnik Asani

Department of Geology
Lund University
2015

Contents

Cover Picture: Overview photo of the drumlin. Photo by Per Möller.

A geophysical study of a drumlin in the Åsnen area, Småland, south Sweden

BESNIK ASANI

Asani, B., 2015: A geophysical study of a drumlin in the Åsnen area, Småland, south Sweden. Dissertations in Geology at Lunds University, No. 444, 32 pp. 15 hp. (ECTS credits)

Abstract: The sediment composition of drumlins in the Åsnen area in Småland, south Sweden is poorly studied. Excavations are being planned with intention to study the internal architecture and composition of these drumlins. As a preliminary investigation this thesis was done to determine the sediment depths in the tail of a drumlin at Rörvik gård, situated on Vemboö in Lake Åsnen. To determine the sediment depths three geophysical methods were carried out on the drumlin: (i) resistivity (cves), (ii) electromagnetic slingram and (iii) induced polarization effect measurements. Using the data acquired from these measurements, models presenting maximum and minimum potential depths to the bedrock were interpreted. The results indicate that the drumlin has varying sediment depths and undulating bedrock with the sediment on top being independent from the form of the bedrock. Sediment depths of 2m to 8m were found in the drumlin according to the minimum interpretation, and depths of 2-15+ m according to the maximum interpretation. Due to equivalence problems that come with the three selected geophysical methods, it is suggested that drilling samples are suited to solve the problem, providing much more accurate interpretations. It is also suggested that the geophysical method seismic refraction studies could potentially be another choice of method to be used in similar studies.

Key words: Geophysics, drumlin, resistivity, induced-Polarization, electromagnetic slingram

Supervisors: Per Möller, Hans Jeppsson

Subject: Quaternary Geology (Geophysics)

Besnik Asani, Department of Geology, Lund University, Sölvegatan 12, 223 62 Lund, Sweden. E-post: bossnik@null.net

Geofysisk undersökning av en drumlin i Åsnenområdet, Småland, södra Sverige

BESNIK ASANI

Asani, B., 2015: Geofysisk undersökning av en drumlin i Åsnenområdet, Småland, södra Sverige. *Examensarbeten i geologi vid Lunds universitet*, Nr. 444, 32 sid. 15 hp.

Sammanfattning: Sedimentkompositionen av drumliner i Åsnenområdet i Småland, södra Sverige är något som är dåligt studerat. Schaktning har planerats med målet att studera den interna arkitekturen och kompositionen av dessa drumliner. Som en preliminär studie har detta examensarbete utförts för att bestämma jorddjup i svansen av en drumlin i Rörvik gård, belägen i Vemboö i sjön Åsnen. För att bestämma jorddjupet användes tre olika geofysiska mätmetoder på drumlinen: (i) resistivitetsmätning (cves), (ii) elektromagnetisk profilering med stångslingram och (iii) inducerad polarisation mätning. Den samlade data från dessa mätningar användes för att tolka fram modeller vilka visar maximal och minimal potentiellt djup till berggrunden. Resultaten indikerar att drumlinen har varierande jorddjup och en undulerande berggrund där formen på jordarterna ovanpå är oberoende av formen av berggrunden. Jorddjup på 2m till 8m finns i drumlinen enligt den minimala tolkingen, och djup på 2m till 15+ m enligt den maximala tolkingen. På grund av ekvivalensproblem vid tolkning av data från de tre valda geofysiska metoderna föreslås att borrprov används för att lösa problemet och ge mer noggranna tolkningar. Det föreslås även att den geofysiska metoden refraktions seismisk vara användbar för liknande studier.

Nyckelord: Geofysik, drumlin, resistivitet, inducerad polarisation, elektromagnetisk profilering, stångslingram

Handledare: Per Möller, Hans Jeppsson

Ämnesinriktning: Kvartärgeologi (Geofysik)

Besnik Asani, Geologiska institutionen, Lunds universitet, Sölvegatan 12, 223 62 Lund, Sverige. E-post: bossnik@null.net

1 Introduction

1.1 Background

Drumlins, forming large tracts of streamlined terrain has since long been described from central parts of Småland (see review in, e.g., Möller (1989)). These come in two types (Möller & Dowling, accepted): as (i) rock-cored drumlins and (ii) as sediment-cored drumlins or larger patches of sorted sediment with a streamlined top surface with a till carapace (Möller and Murray, accepted). Rock-cored drumlins are totally predominating within and around Lake Åsnen, having an oval plan form with a blunt stoss end and a tapering off tail in the former ice-flow direction, and with mean height/width of 6.3 and 320 meters, respectively (Möller & Dowling, accepted). LiDAR-derived hill shade terrain models suggest that bedrock cores are exclusively located in the stoss end of the drumlins. The frequency of (exposed) bedrock cores in mapped drumlins is presently investigated by Zaman (2015) for two field-check areas in the Lake Åsnen district The internal architecture, sediment composition and relation to bedrock in a wider context of these drumlinoid landforms around Lake Åsnen have not yet been studied. However, there are plans to excavate and study the internals of drumlins around Lake Åsnen and this thesis is a preliminary investigation in such a context of future possible excavations. This investigation is a geophysical study of one bedrock-cored drumlin at Rörvik gård, situated on Vemboö in Lake Åsnen (Fig. 1).

Fig. 1. A map of southern Sweden and a zoomed map showing the study location marked in black. Map of Sweden from Wikipedia and map of study location from Lantmäteriet.

1.2 Aim of the study

By measuring the resistivity, induced polarization and apparent conductivity on the drumlin, a model of the internal architecture, showing bedrock and sediment will be made. The model will suggest sediment depths to the bedrock.

1.3 Geological background

According to the Swedish Geological Survey (SGU) map in Wik et al. (2009), two types of bedrock have been interpolated through the drumlin at Rörvik gård, one being felsic plutonic rock, and the other felsic extrusive rock (Fig. 2). It was also mapped in SGU's maps on Quaternary deposits that the drumlin merely consists of an undifferentiated till. Sedimentological studies carried out at Horgeboda, which is approximately 10 km southwest of the study location, in transverse to ice-flow moraine ridges (Åsnen-type ribbed moraine; Möller (2010)) show that these consist of silty-sandy, gravelly-sandy and sandy gravelly diamicts with high lithology percentage in the clasts from the local bedrock. These results could potentially indicate similar till in the drumlin at Rörvik gård.

1.4 Methods

Three geophysical methods were used. (i) Resistivity and (ii) induced polarization (IP) measurements with the use of the instrument ABEM Terrameter LS, and (iii) measurement of electromagnetic waves' real and imaginary parts with the use of the instrument Ge-

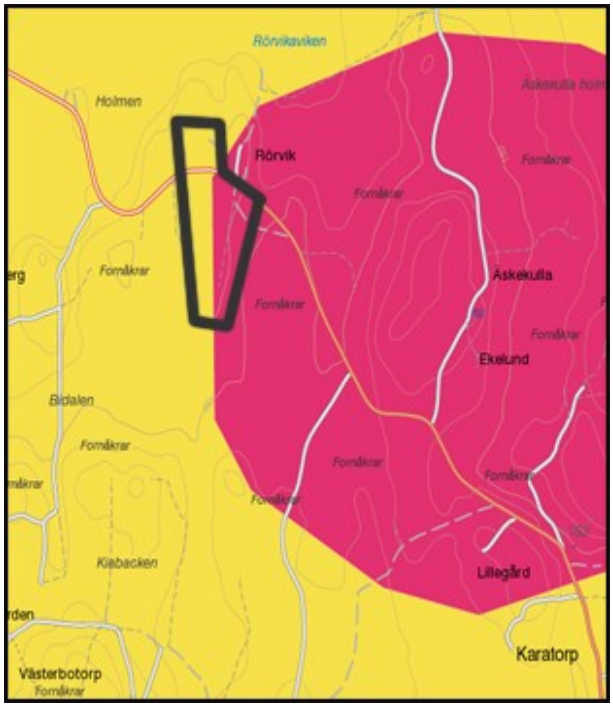

Fig. 2. SGU bedrock map 1:1 million showing the felsic extrusive rock as yellow and felsic plutonic rock as pink. The study area is inside the black polygon.

ophex GEM-2 Ski. The resistivity and IP data were topographically adjusted in Microsoft Excel with GPS data gathered with the use of TOPCON GPS GR-5 and FC336 and then inverted with the use of the software RES2DINV. The topography-adjusted data was later plotted in the software Erigraph. The electromagnetic data was recalculated into apparent conductivity in the software EMInvertor and then adjusted in Microsoft Excel to be plotted in a map with use of the software Surfer 12. Adobe Illustrator and Photoshop were used to make the geological models.

2 Geophysical methods

2.1 Resistivity measurement (CVES) theory

2.1.1 Electrical resistivity

Ohm's law states that the potential difference (V) in a conducting object is equal to the electrical current (I) multiplied with the resistance of the conductor (R) (Lowrie, 2007).

$$V = IR$$

In one dimensional conducting objects, resistance is equal to the material property resistivity (ρ) multiplied with the geometrical factor, which is the length of the object (L) divided by the cross-sectional area (A) (Lowrie, 2007; Jeppsson & Dahlin, 2015a). Resistivity is the "*ability to oppose a flow of charge"* and is measured in Ohm-meter (Ωm) (Lowrie, 2007; Jeppsson & Dahlin, 2015a).

$$R = \frac{\rho L}{A}$$

In the formula of resistance, resistance could be rewritten into V/I, and then in another step be rearranged.

$$\frac{V}{I} = \frac{\rho L}{A} \longrightarrow \frac{V}{L} = \frac{\rho I}{A}$$

V/L is *"the force that the electric field exerts on a charge*" (E), and I/A the current density (J) (Jeppsson & Dahlin, 2015a). By rearranging the units in the formula, it can be concluded that resistivity is equal to the electric field (E) divided by the current density (J).

$$\rho = \frac{E}{J}$$

During resistivity measurements two electrodes conduct an adjusted flow of electrical current into the ground. The adjustment is handled by the terrameter through controlling the potential difference between the two electrodes (Jeppsson & Dahlin, 2015a). The conduction of electricity into the ground causes a three dimensional electric potential field (Jeppsson & Dahlin, 2015a). Two other electrodes measure the potential difference in two points (Fig. 3). By knowing the electrical current and potential difference the resistance can be calculated. Since the conducting object is a three dimensional object and not a metal wire, the geometrical factor (G) is not L/A (Jeppsson & Dahlin, 2015a).

$$\rho = RG$$

The formula to calculate the resistivity with a three dimensional geometrical factor is presented in Jeppsson & Dahlin (2015a). The formula results in:

$$\rho = RG = R\,\frac{2\pi}{\left[\left(\frac{1}{r_A} - \frac{1}{r_B}\right) - \left(\frac{1}{R_A} - \frac{1}{R_B}\right)\right]}$$

, where r_A and R_A are the distances from the two potential difference electrodes to the positive current electrode, and r_B and R_B the distances to the negative current electrode.

2.1.2 Investigation depth

The practical depth penetration of electricity being conducted in the ground is defined by the depth that 50 % of the current reaches (Jeppsson & Dahlin, 2015a). According to Jeppson & Dahlin (2015a) the investigation depth is dependent on three factors:

- distance between the current electrodes,
- the electrode configurations, and,
- the geological units' properties.

The investigation depth increases with distance between the current electrodes, and is estimated to reach approximately a depth equal to a third of the distance between the midpoint and the furthest current electrode (Jeppsson & Dahlin, 2015a). There are different electrode configurations, with each having its strengths and weaknesses. The electrical current concentrates in conductive geological units and can decrease the investigation depth if the underlying geological unit has high resistivity (Jeppsson & Dahlin, 2015a).

2.1.3 Apparent resistivity

When conducting resistivity measurements, it is assumed that the ground is homogenous which, is not the case in most environments (Jeppsson & Dahlin, 2015a). The terrameter measures a mean resistivity from more than one geological unit and the measurement is affected by surrounding heterogeneities, producing data that come out as the "apparent resistivity" (Jeppsson & Dahlin, 2015a; Lowrie, 2007). Apparent resistivity is implausible for geological interpreta-

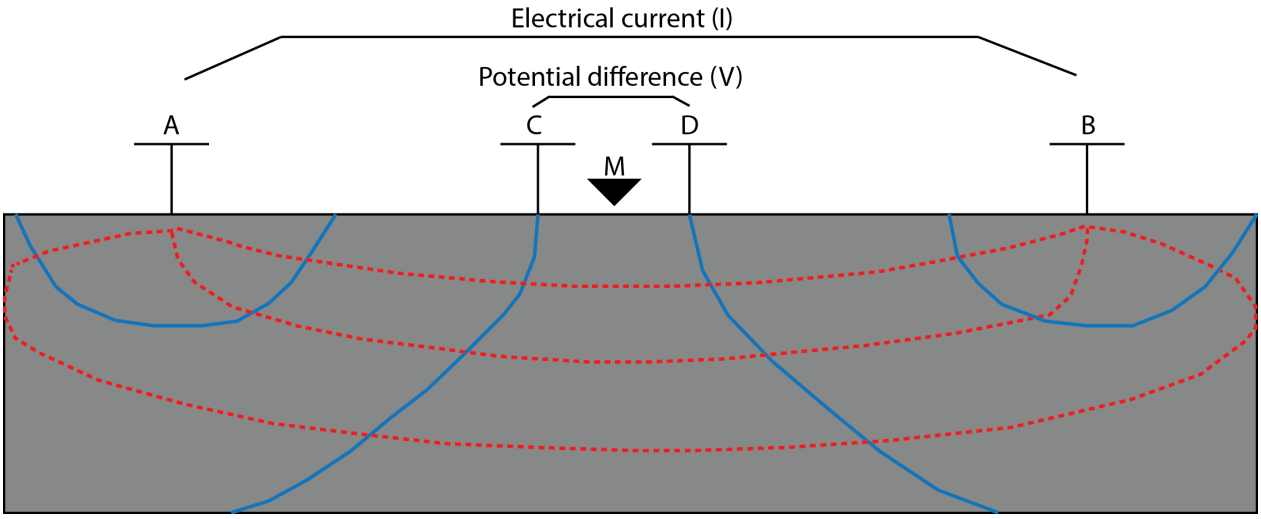

Fig. 3. The basics of resistivity measurements. A and B are current electrodes. C and D are potential difference electrodes. M is the point of measurement. Dashed lines indicate current flow and blue lines electric field potential. The figure is based on work

tion; it is therefore processed through an inversion process in computer programs (Jeppsson & Dahlin, 2015a; Lowrie, 2007). The inversed data is usable for geological interpretation (Jeppsson & Dahlin, 2015a).

2.1.4 Inversion

A pseudo section is the result of a resistivity measurement (Fig. 4) and is not plausible data to be used for geological interpretation since it presents the apparent resistivity. To attribute real resistivity to different parts and geological units of the resistivity section, an inversion has to be carried out which creates an inverted section (Fig. 5). This is done by assuming a starting model, and calculating what pseudo section the model would result in and then compare it with the measured pseudo section and successively adjust the model until there is a minimal difference of around 2 % (Reynolds, 1997; Jeppsson & Dahlin, 2015a; Barker, 1992; Zohdy, 1989).

2.1.5 Resolution

The ability to distinguish between geological units in a resistivity section is dependent on four factors according to Jeppsson & Dahlin (2015a):

- electrode configuration,
- geometry and size of geological units,
- resistivity contrast between geological units, and,
- distance between electrodes.

The different electrode configurations have their strengths and weaknesses regarding vertical and horizontal resolution. Small geological units at greater depths will have low resolution and might not be distinguished from its surroundings (Jeppsson & Dahlin, 2015a). Higher resistivity contrasts increase the resolution. Larger distance between the electrodes means

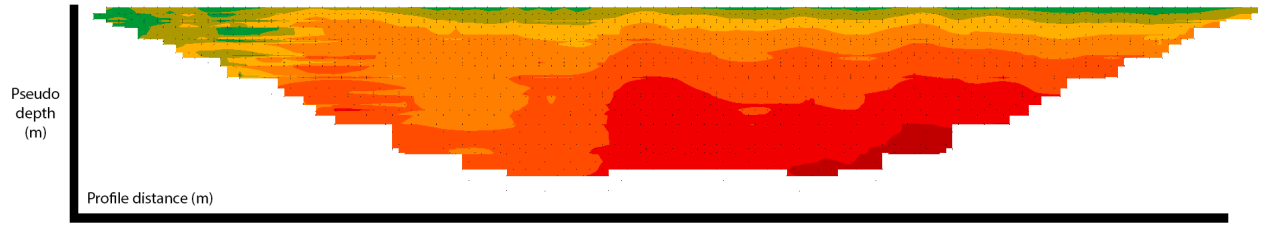

Fig. 4. A resistivity pseudo section showing different apparent resistivity values with pseudo depths.

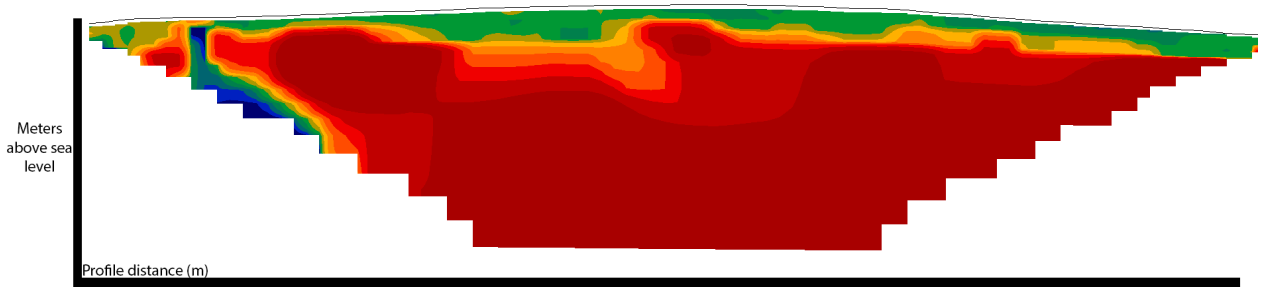

Fig. 5. The result of inversion of Fig. 4. Inverted resistivity section showing resistivity values with real depths.

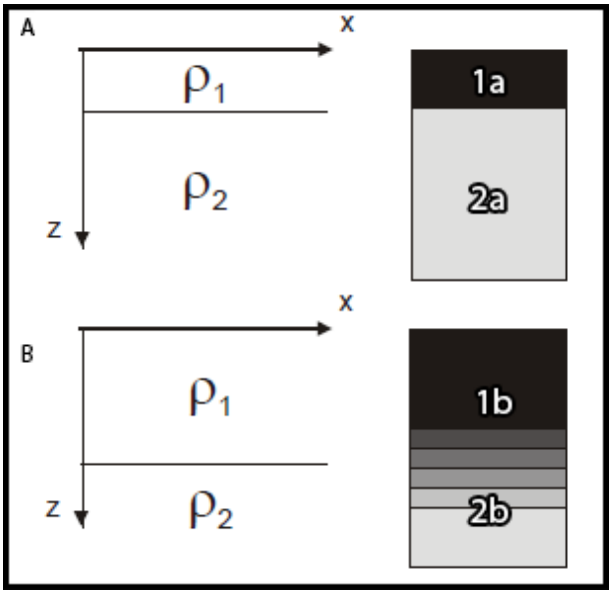

Fig. 6. A) Two geological units with different resistivity values at a smaller depth, resulting in a clear boundary in the resistivity section. B) The same two geological units but the boundary at a greater depth, resulting in a gradational boundary in the resistivity section. The figure is based on work by

larger depth of penetration but less resolution (Jeppsson & Dahlin, 2015a). The effects of lower resolution can be seen in Fig. 6.

2.1.6 Resistivity of geological material

Electric current can be conducted through sediment and rock in three different ways according to Lowrie (2007), Reynolds (1997) and Jeppsson & Dahlin (2015):

- ohmic conduction,
- dielectric conduction, and,
- electrolytic conduction.

Ohmic conduction is found in metals where the electrons drift freely and collide with the atoms causing them to scatter randomly (Lowrie, 2007). When an electrical field has been applied, the free electrons are transported in the direction of the field (Lowrie, 2007). The resistivity is dependent on the frequency of collisions, where high frequencies of collisions result in high resistivity (Lowrie, 2007). Dielectric conduction is the form of conduction in insulators such as most rock (Lowrie, 2007; Reynolds, 1997). The electrons are not free, but bound to the atoms' nuclei (Lowrie, 2007). When an electrical current is conducted through such a material, the electrons are slightly shifted in regard to the protons (Lowrie, 2007; Reynolds, 1997). Electrolytic conduction is the form of conduction found in aqueous solutions and occurs by slow movement of the ions (Lowrie, 2007; Reynolds 1997).

Dielectric conduction is the primary form of conduction in geological material, and depends on the

Table 1. Resistivity intervals of geological material, based

Geological material	Resistivity interval (Ωm)
Clay	1-100
Dry sand	800-5000
Wet sand	100-500
Clay-rich till	20-200
Clay-poor till	300-3000
Bedrock	2000-50000
Weathered bedrock	200-4000

porosity, amount and type fluid in the different geological units (Jeppsson & Dahlin, 2015a). The presence of groundwater in resistivity sections can cause a noticeable resistivity contrast between the sediment above and beneath the groundwater level (Jeppsson &, Dahlin 2015a). The surfaces of clay minerals are negatively charged and cause positively charged ions to bind to their surfaces (Jeppsson & Dahlin, 2015a). This gives rise to diffuse double layer and shows a significant decrease in resistivity in material consisting of clay minerals (Jeppsson & Dahlin, 2015a).Weathered rock with clay minerals will have a resistivity contrast to its surrounding fresh rock (Jeppsson & Dahlin, 2015a).

Different geological material show different resistivity intervals and can be used for interpretation (Table 1). Some resistivity intervals do overlap with each other, making a geological interpretation unreliable unless compared to other data such as drilling samples and other geophysical methods, etc.

2.1.7 Configurations and multi-electrode resistivity

There are several ways the two sets of current and potential difference electrodes can be setup, such as the wenner, schlumberger and dipole-dipole set-ups. In this study the gradient configuration was used, which is an asymmetrical variant of the schlumberger configuration (Fig. 7). It is the most suitable configuration

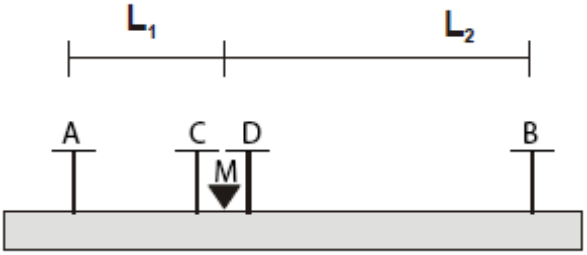

Fig. 7. The gradient configuration. A and B are current electrodes, with different distances to the point of measurement M. C and D are the potential difference electrodes and both have the same distance to the measuring point. Based on

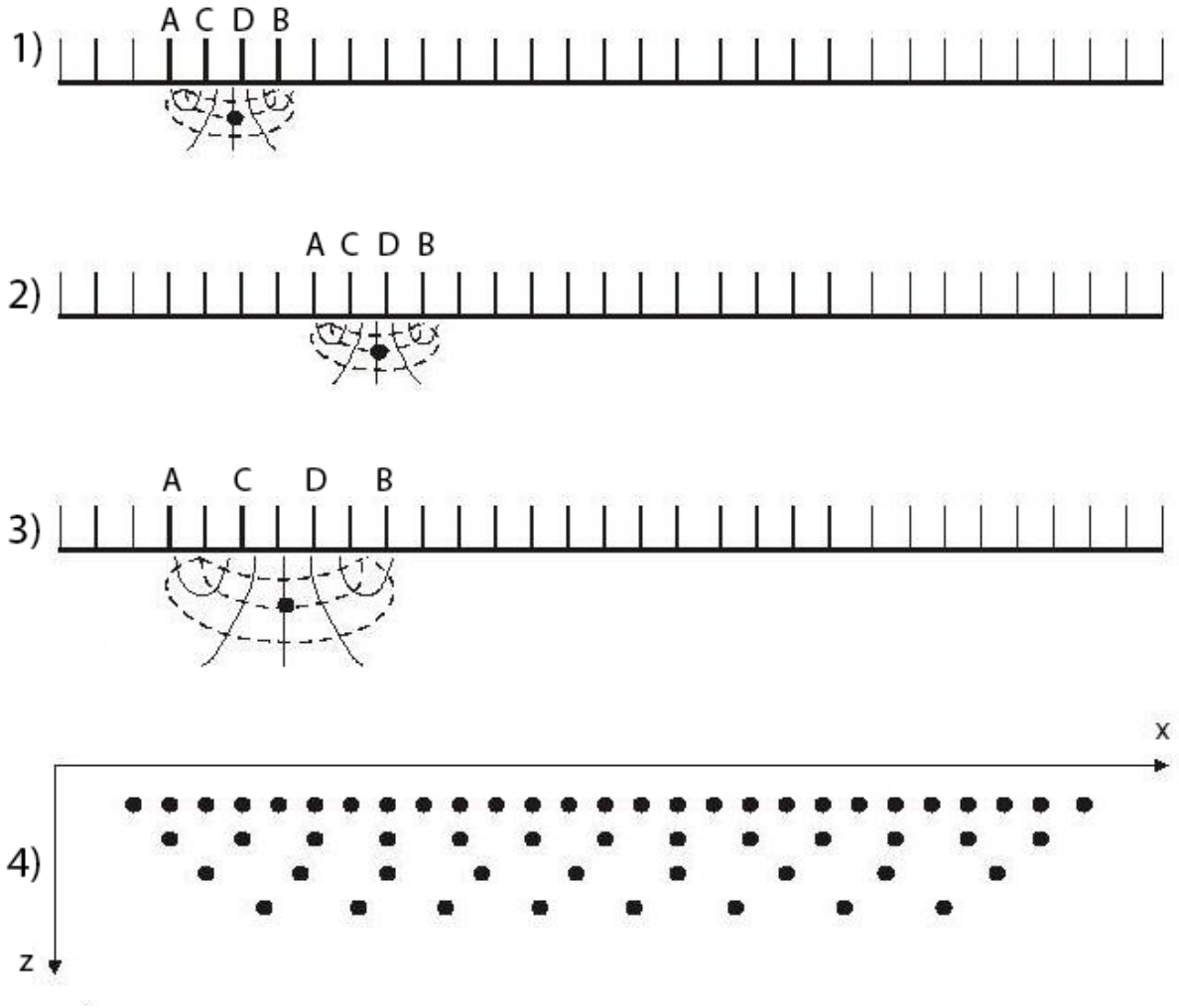

Fig. 8. Multi-electrode measurement. A and B represent the current electrodes and C and D the potential difference electrodes. The dots represent a measurement point. Based on work by Jeppsson & Dahlin (2015a).

for multi-electrode measurements as it allows most measurements to be carried out simultaneously (Jeppsson & Dahlin, 2015a; Lowrie, 2007).

The most common type of resistivity setup is the multi-electrode setup, which was used in this study. Instead of using only 4 electrodes and systematically moving them in a profile, up to 81 electrodes are placed and connected with the terrameter through a cable system. This makes the process automated and several measurements are carried out simultaneously with different distances between the electrodes to the measuring points (Fig. 8). This results in many measuring points with varying resolution and penetration depths (Jeppsson & Dahlin, 2015a).

2.2 Electromagnetic slingram measurement theory

2.2.1 Electromagnetic waves

An electromagnetic wave is the transport of energy by the coupling and interaction of electrical and magnetic fields (Lowrie, 2007; Jeppsson & Dahlin, 2015b). The waves are made up by two orthogonal vector components, the electric intensity field vector (E) which is measured in V/m, and the magnetizing force field vector (H) which is measured in A/m (Lowrie 2007; Jeppsson & Dahlin, 2015b; Reynolds, 1997). The energy between the two vectors is equally divided (Lowrie 2007; Jeppsson & Dahlin, 2015b; Reynolds, 1997). Electromagnetic waves are formed in two ways according to Maxwell's equations as described in Jeppsson & Dahlin (2015b): "*an alternating electrical field gives rise to an alternating magnetic field, and an alternating magnetic field gives rise to an alternating*

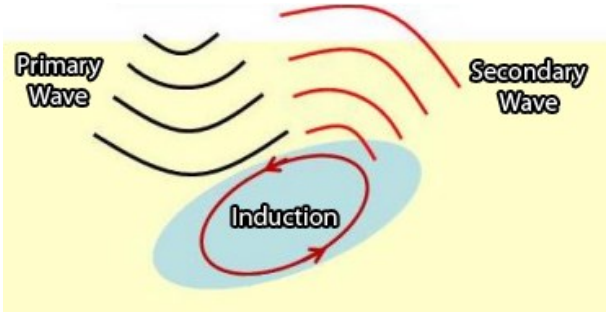

Fig. 9. Illustration of induction of an object giving rise to a secondary wave. Based on work by Jeppsson & Dahlin

electrical field". This phenomena causes induction in conducting material when being exposed to alternating magnetic fields. The induction in the material gives rise to new induced electromagnetic waves that do not share the same properties as the primary wave (Fig. 9) (Jeppsson & Dahlin 2015b; Lowrie, 2007). The induced secondary magnetic field consists of two components, one real and one imaginary part (Jeppsson & Dahlin 2015b). In a vector diagram showing the primary and induced secondary magnetic field, the real part of the secondary field is the part that is in phase with the primary field, and the imaginary part is the part that is phase shifted 90° in regard to the primary field (Jeppsson & Dahlin, 2015b). The sizes of these parts are dependent on the conductivity of the material (Jeppsson & Dahlin, 2015b).

2.2.2 Penetration depth

In this study the instrument Geophex GEM-2 Ski was used, which consists of a coil that transmits the primary field and another coil that receives the total wave that includes both the primary and secondary wave. Electromagnetic waves are attenuated with time due to energy loss (Jeppsson & Dahlin, 2015b). Skin depth (δ) is the depth where the wave has been attenuated to approximately 37 % of its original amount of energy, and is dependent on the resistivity (ρ) and frequency (*f*) used (Jeppsson & Dahlin, 2015b). Higher frequencies used and conductivity of the geological units leads to more attenuation (Fig. 10) (Jeppsson & Dahlin, 2015b). A rule of thumb is that the practical penetration depth is around a 1/5 of the skin depth (Jeppsson & Dahlin, 2015b; Lowrie 2007).

$$\delta = 503\sqrt{\frac{\rho}{f}}$$

2.2.3 Conductivity measurement

An induction number is the transmitter-receiver length divided by the skin depth (Jeppsson & Dahlin, 2015b). If the induction number is low, the magnitude of the imaginary part in the secondary wave is only dependent on the conductivity of the geological units (Milsom & Eriksen, 2011). This can be used to recalculate the imaginary part of the secondary waves into apparent conductivity, measured in mS/m (Jeppsson & Dahlin, 2015b; Milsom & Eriksen, 2011).

2.3 Induced polarization measurement theory

2.3.1 Induced polarization

When electricity is being conducted in the ground there is a sudden increase in the voltage (V_i) which then is gradually increased until the voltage reaches a maximum value of (V_{max}). The same applies when the conduction of electricity to the ground is stopped; then

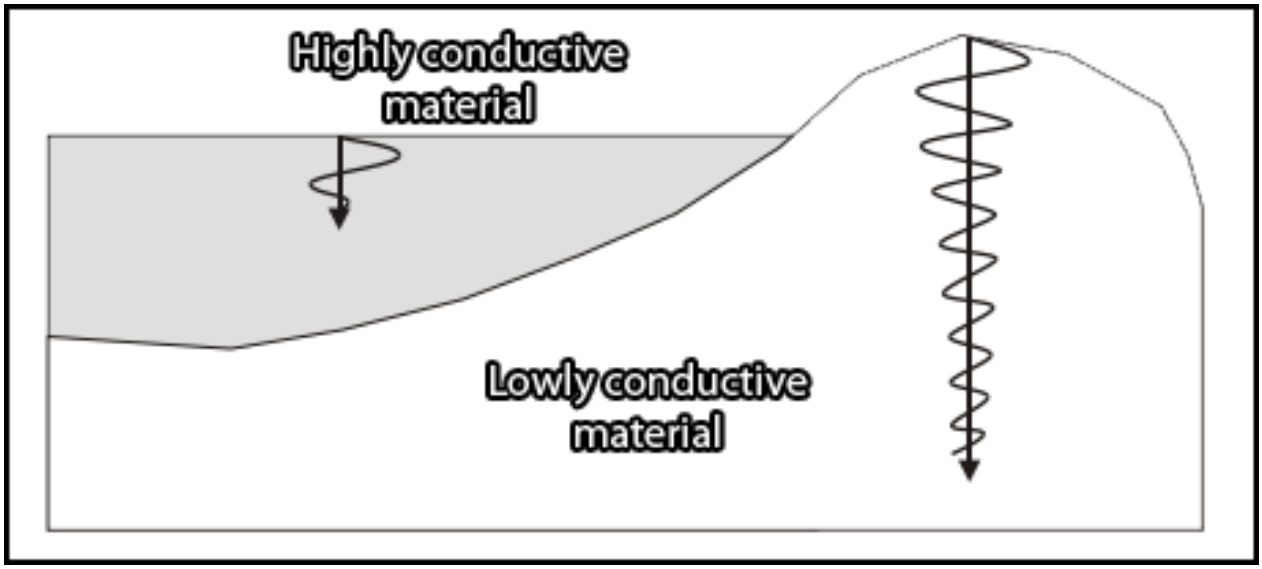

Fig. 10. Illustration of attenuation and depth penetration of electromagnetic waves in different geological material with different conductivity. Based on work by Jeppsson & Dahlin (2015b).

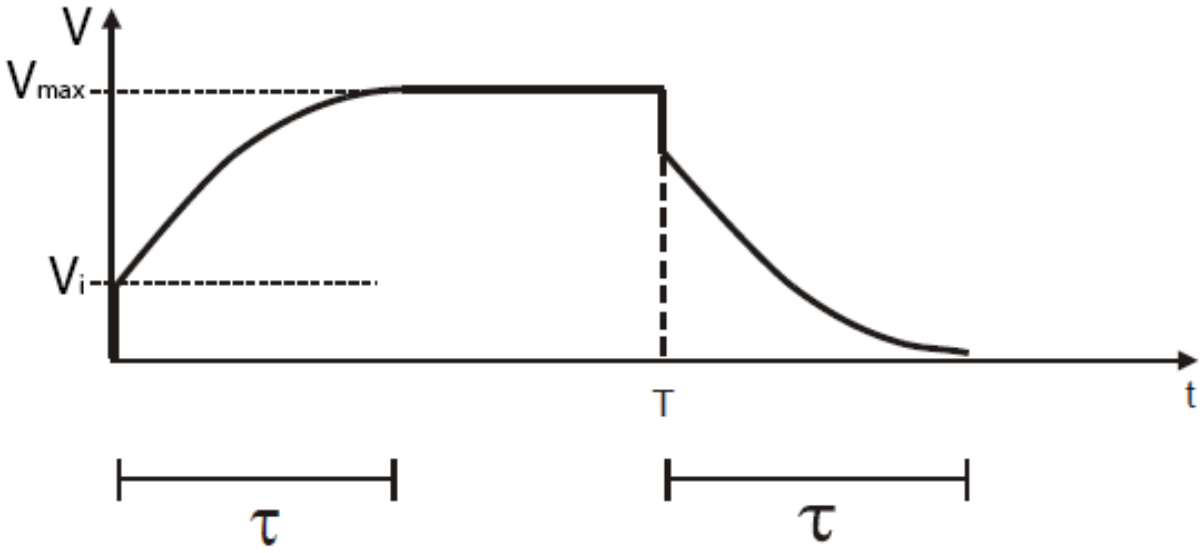

Fig. 11. A diagram showing the IP-effect. Voltage on the Y-axis and time on the X-axis. Based on work by Jeppsson & Dahlin (2015a).

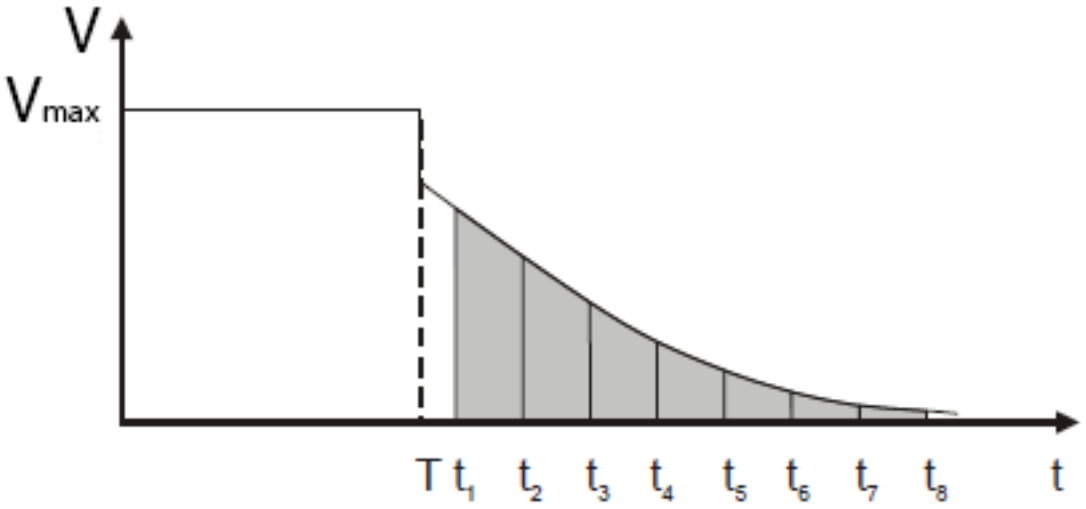

Fig. 12. Delay time divided into several IP-windows. Based on work by Jeppsson & Dahlin (2015a).

there is a sudden decrease in voltage (V_i) and, concordantly, a gradual decrease of the voltage (Lowrie, 2007; Jeppsson & Dahlin, 2015a). The time for the gradual changes in voltage to reach (V_{max}), or original voltage, is called delay time (τ) (Fig. 11); this is the so called Induced Polarization effect (IP-effect) (Lowrie, 2007; Jeppsson & Dahlin, 2015a).

The IP-effect is explained by two main mechanisms, the membrane polarization and electrode polarization (Milsom & Eriksen, 2011). Membrane polarization occurs when electrolytes in small pore spaces in rock are exposed to an electrical field (Jeppsson & Dahlin, 2015a). Clayey and platy minerals tend to have negatively charged surface layers, in which the positive ions of the pore fluid form an immobile layer which tend to block nearby pores (Lowrie, 2007; Jeppsson & Dahlin, 2015a; Milsom & Eriksen, 2011). As explained in Lowrie (2007): "*When an external voltage is applied, positive ions can pass through the "cloud" of positive charge but negative ions accumulate, unless the pore size is large enough to allow them to bypass the blockage. The effect is like a membrane, which selectively allows the passage of one type of ion. It causes temporary accumulations of negative ions, giving a polarized ionic distribution in the rock*". Ions in the fluid will neutralize the oppositely directed field formed by the polarization, which will allow the voltage to reach a maximum (Jeppsson & Dahlin, 2015a). When the external voltage is no longer being applied, the polarization is reversed and the ions return to their original positions (Lowrie, 2007; Jeppsson & Dahlin, 2015a; Eriksen & Milsom, 2011). Electrode polarization occurs in material with free electrons and is caused by external electrical fields being applied to

Table 2.Chargeability in milliseconds with integration time of 0.02-1 s. The values and their geologic interpretation are

Geological material	Chargeability (ms)
Shale	50-100
Granite	10-50
Gneiss	6-10
Weathered gneiss	5-30
Till	1-10
Sand and gravel	1-10
Weathered bedrock containing clay	200-4000

the material, causing the electrons to move and polarize (Jeppsson & Dahlin, 2015a). This causes ions surrounding the material to attract and form an oppositely directed field which with time will be neutralized, then allowing the voltage to reach a maximum (Jeppsson & Dahlin, 2015). In IP-effect measurements the chargeability (M) is measured, which is an area in a voltage diagram between two times during the delay time (Fig. 11) (Jeppsson & Dahlin, 2015a). It is measured in mV/V and the formula for chargeability in mV/V is according to Jeppsson & Dahlin (2015a):

$$M = \frac{1}{V_{max}\ (t_2 - t_1)} \int_{t_1}^{t_2} \Delta V(t)dt$$

The delay time can be divided into many time periods and all be used to measure chargeability, giving better information. These are called IP-windows (Fig. 12).

The IP-effect can be measured together with resistivity measurements, since both of them use the same setup with two current electrodes and two potential electrodes with a terrameter.

2.3.2 IP-effect in geological material

The IP-effect can be calculated in milliseconds and mV/V. When measured in mV/V with an integration time of around 1 s, the two different units are interchangeable. In this study the integration time was around 0.96 s and values gathered in mV/V can also be considered interchangeable with ms.

3 Study methodology

3.1 Resistivity and IP-effect measurements

3.1.1 Profiles

Five profiles were laid out over the Rörvik gård drumlin for resistivity and IP-effect measurements. Four of these profiles (profiles 1-4, Fig. 13) are cross profiles over the distal tail of the drumlin and one (profile 5, Fig. 13) is a length profile along the crest line of the drumlin. Profile 1-4 have east to west direction, and profile 5 a north to south direction. GPS data was gathered for every electrode, which is approximately at every 2 m of the profiles, providing altitude and coordinates. The GPS data

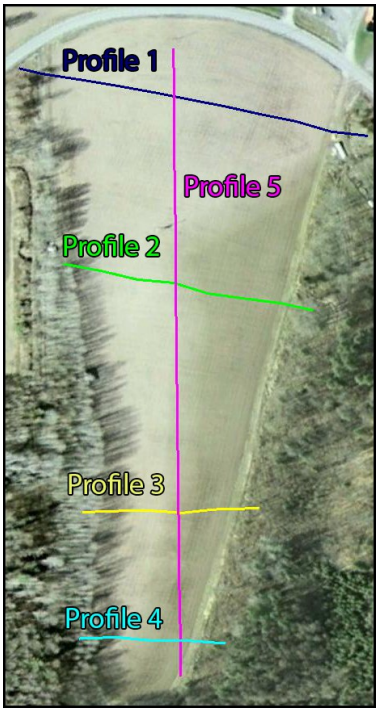

Fig 13. Location of resistivity and IP-effect profiles, laid out over the Rörvik gård drumlin. GPS data were plotted in

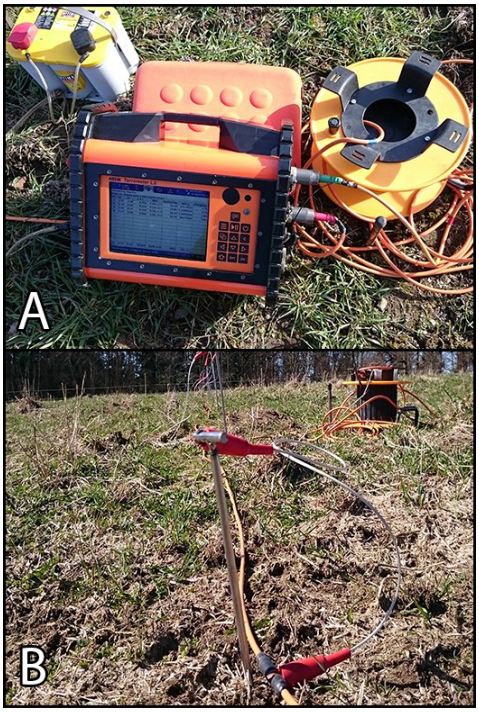

Fig. 14. Equipment used. A) Car battery to the left of the picture, terrameter in the middle and a cable set to the right. B)

was gathered using the devices TOPCON GPS GR-5 and FC336.

3.1.2 The field work

At start, four 40 m long cable sets with electrode distances of 2 m were rolled out along a profile. An electrode pole was pressed into the ground at every 2 m interval and connected to the cable with jumpers (Fig. 14). The terrameter and a car battery were connected at the end of the first cable and then the first measuring sequence was carried out on the three first cables. The fourth cable was not used in the first measurement sequence of a profile, this to increase the amount of measurement points in the beginning of the profile. Each measurement sequence gave around 450-700 readings in total. After the first measurement sequence of a profile was finished, the fourth cable was connected, and the terrameter and car battery were moved up to the middle of the four cable sets, and then a new measurement sequence was started. When the second measuring sequence was finished the first cable was disconnected and moved up in the profile, to become the fourth cable set in the next measurement, and the terrameter and car battery were moved to the middle of the four cable sets. This procedure was repeated until the end of the profile has been reached by the fourth cable set, which was then finished by a last measurement sequence where only 3 cables were used like in the first measurement in the profile, but the terrameter and car battery was then connected in the end of the second cable. The IP-effect was measured simultaneously during resistivity measurement sequences, and used the same setup with 81 electrodes and cable sets.

3.1.3 Data processing

The data collected was altitude adjusted with the GPS data, and that later underwent an inversion process in RES2DINV, after which it was handled in Erigraph to be used for interpretation.

Fig 15. Measurement methodology used in this study for the slingram measurements, by moving from start to end accord-

3.2 Electromagnetic slingram measurements

3.2.1 Profiles

The drumlin ridge was also covered with the slingram measurements. This was carried out by walking across the length axis of the drumlin ridge at varying distances between the slingram profiles, ranging from approximately 5 to 15m (Fig. 15). Slingram measurements were also done on the north to profile 1, i.e. north of the crossing road (Fig. 2 and 13) where bedrock is exposed above ground surface, this to give an indication of what conductivity is the bedrock.

3.2.2 The field work

The measurements were done by carrying the instrument across the study area, covering as much ground as deemed needed. During measurements the instrument recorded over several frequencies (18125Hz, 35025Hz and 63375Hz) as different frequencies give different resolutions and penetration depths (Hauck & Kneisel, 2008). The slingram has an inbuilt GPS but creates a local coordinate system.

3.2.3 Data processing

The data collected was converted from real and imaginary parts into apparent conductivity, using EMInvertor by GEM, and later adjusted in Microsoft Excel to be used in the mapping software Surfer 12.

4 Results

4.1 Methodology of interpretation

Each measured profile has its' resistivity and IP-effect presented together with a section showing interpreted bedrock. Using the interpreted section, maximum and minimum depths are calculated for the different profiles. The IP-effect data shows very low values throughout all sections, especially in profile 2 and 3 where values are ≤0.9mV/V. With such low values it is not possible to distinguish between bedrock and sediment. Bedrock is known to be present from the resistivity measurements with resistivity values >10000Ωm in profile 2 and 3, but in spite of this no contrast is seen in the IP-effect values. The IP-effect data has therefore not been used to interpret location of bedrock. It was however used to interpret fractures in rock and anomalies caused by disturbing objects. Weathered rock tends to show higher IP-effect values (Jeppsson & Dahlin, 2015a). Therefore, when resistivity anomalies have been observed, such as in profile 1, the IP-effect data was used to interpret the cause of the anomaly. Electromagnetic slingram measurement was done on exposed bedrock to get apparent conductivity values of the local bedrock, which is around 0.1 mS/m,

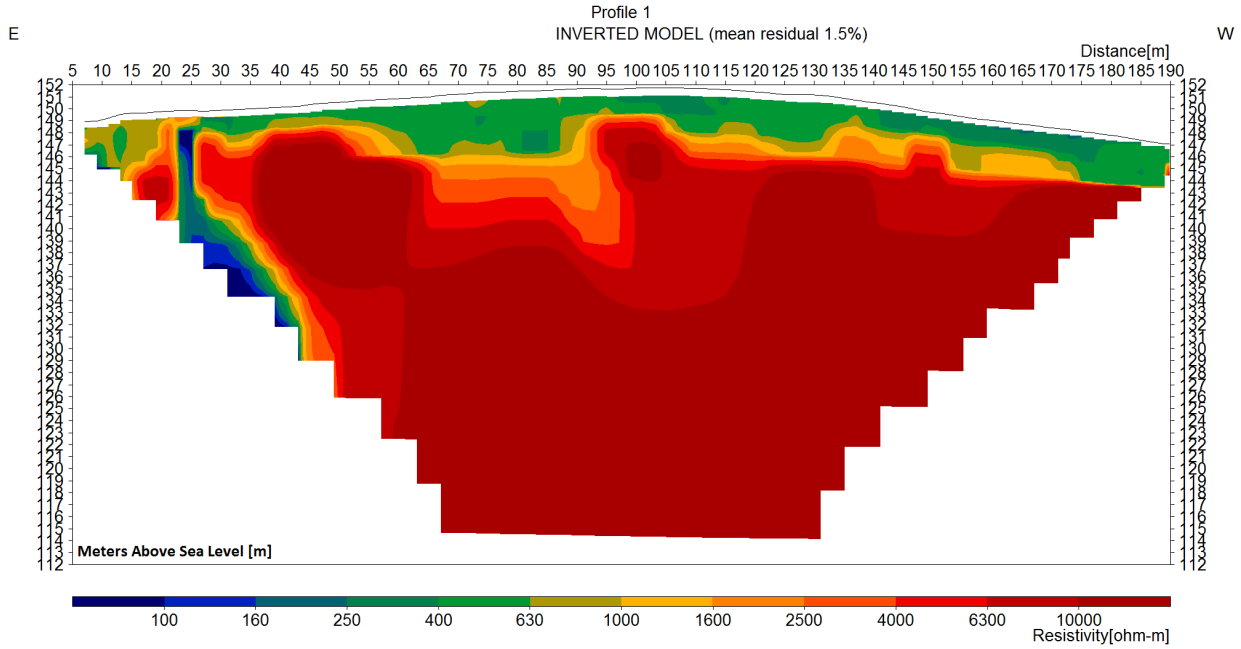

Fig 16. Resistivity section of profile 1.

and values observed in the drumlin close to 0.1 mS/m will be assumed to have smaller sediment depths. Higher apparent conductivity values, such as 3mS/m, are interpreted as indications of relatively larger sediment depths. Since there was no drilling data to correlate the slingram data with, it is merely an indicator of relative depth and was used to strengthen interpretations of sediment depths from resistivity data. This leaves the resistivity data as the core of the interpretations made.

Resistivity sections are limited to show values from 0 to 10000Ωm divided up in a legend that shows 12 colours in the software Erigraph and attributing one colour to each interval of resistivity values. By limiting all measurements above 10000Ωm to one maximum value, the 12 colours will display smaller resistivity intervals. A difference in resistivity between 10000Ωm and 20000Ωm is judged to be of minor importance for the type of interpretations done in this study, as they both indicate bedrock according to Jeppsson & Dahlin (2015a). Each IP-effect section has its own legend limited to its minimum and maximum chargeability. The resistivity values in Tables 1 and 2 have been used as guidelines for attributing different geological material to different resistivity and IP-effect values. As seen in Table 1, the resistivity values of some sediment types and bedrock overlap, and can have very large intervals. As an example, bedrock can have values from 200Ωm up to 50000Ωm, depending if it is weathered or not in the upper part. This means that a certain resistivity value can be the same for several types of geological material. A resistivity value of 1800Ωm could according to Table 1 represent dry sand, non-clayey till or bedrock. As there is no drill data or sections in the drumlins to use for "calibrating" the resistivity data, they can only be classified as representing sediment or not (i.e. bedrock), with no further subdivision into different types of sediment.

For the resistivity interpretation, all resistivity values above 3000Ωm have been classified as confirmed bedrock, and values under 1600Ωm as undifferentiated sediment. This leaves a gap from 1600 to 3000Ωm, for which it is unclear whether it is more likely bedrock or sediment. If not "*geological common sense*" suggests one or the other, strata or section parts with such an resistivity interval has been classed as indistinguishable. If this is the case over parts of the sections, this means that the boundary between bedrock and sediment could be anywhere in that zone with maximum depth being the depth if the indistinguishable zone is entirely sediment, and minimum depth if the indistinguishable zone is entirely bedrock. The true value could be anywhere in-between. In some profiles there are very low resistivity values in relation to the bedrock, but seen to cut through bedrock at large depths. These units have been marked as anomalies. These can either be caused by disturbing objects, or increased conductivity from weathered rock. Weathered rock can contain more fluids in comparison to fresh rock, and therefore has lower resistivity (Jeppsson & Dahlin, 2015a).

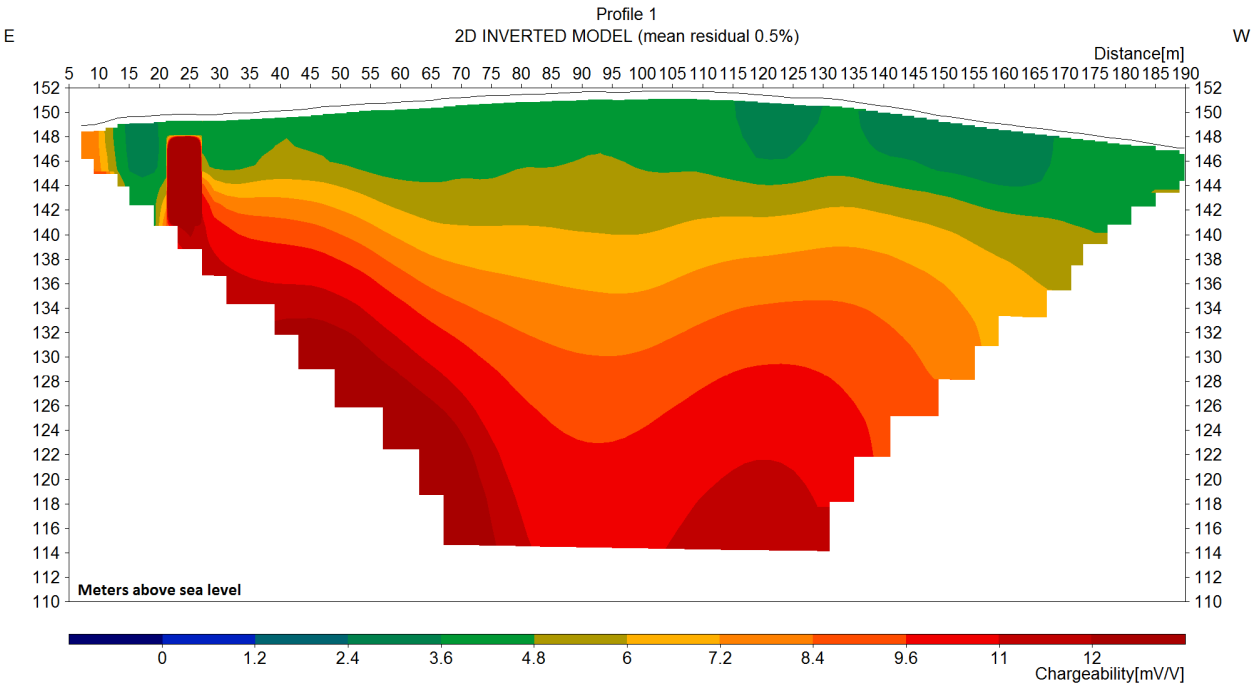

Fig 17. IP-effect section of profile 1.

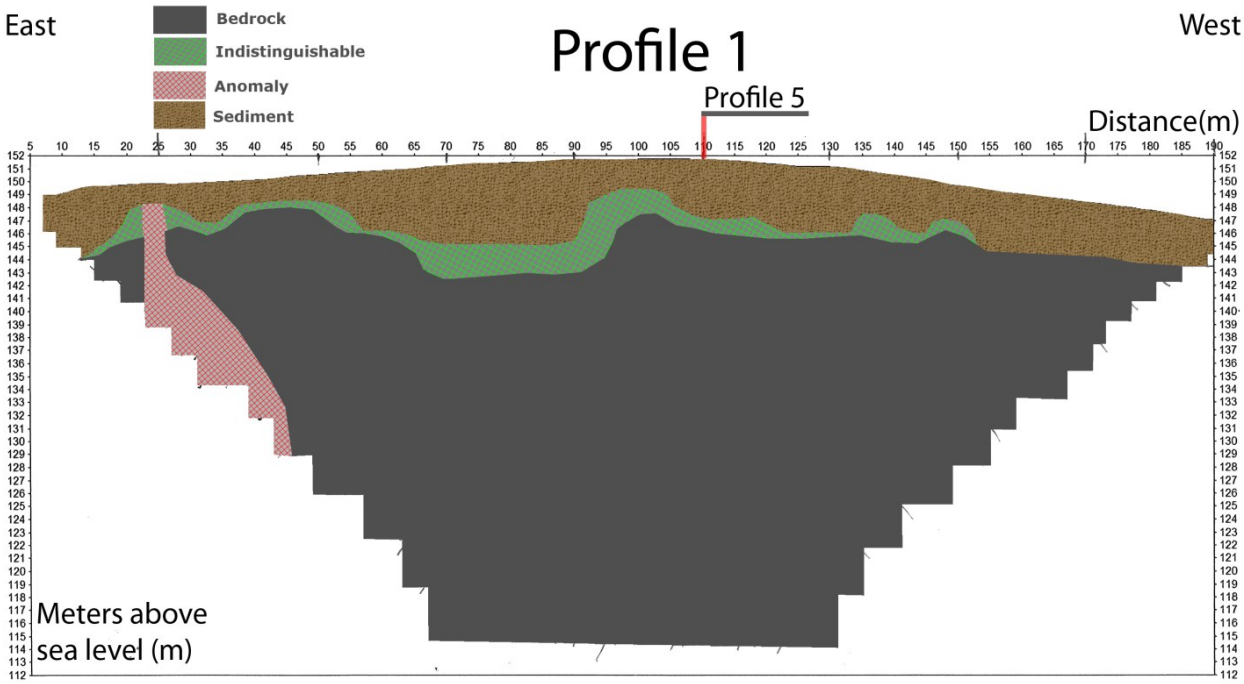

Fig 18. An interpreted geological model of profile 1. At 110 m a red line marks the crossing with profile 5. The unit marked as bedrock is very likely bedrock, and the unit marked as sediment is very likely such, based on their high versus and low resistivities, respectively (Table 1).The units marked 'indistinguishable' and 'anomaly' are zones where the bedrock and sediment could

Table 3. The interpreted maximum and minimum thickness of sediment down to bedrock along profile 1. The (*) marks the thickness of sediment at the 110 m mark, which is the crossing point with profile 5 in which no 'indistinguishable' zone recorded, which makes this thickness value more likely.

Distance (m)	30	50	70	90	110	130	150	170	190
Max (m)	3	3	8	8	5	5	4	4	4
Min (m)	3	2	6	6	4*	5	2	4	4

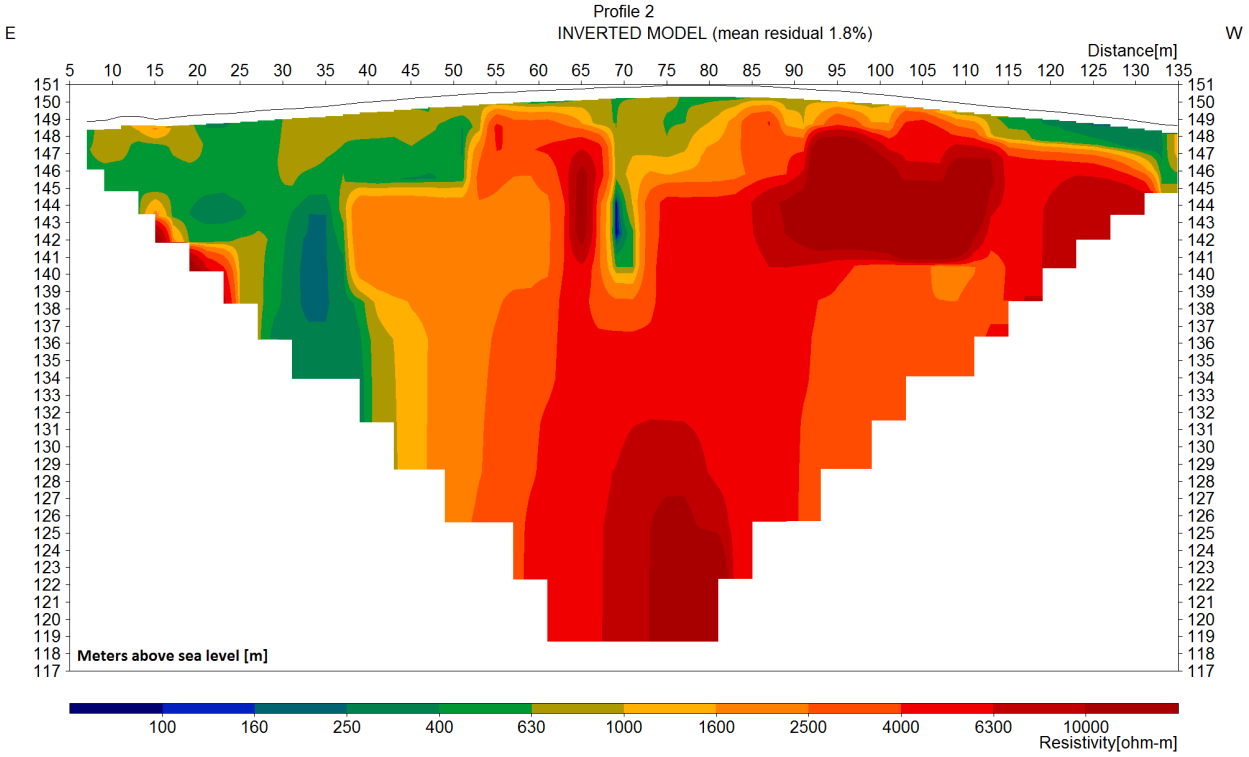

Fig 19. Resistivity section of profile 2.

4.2 Resistivity and IP-effect results

4.2.1 Profile 1

4.2.1.1 Inverted models

Profile 1 (Fig. 13) measures 196 m in length, over which the maximum measurement depth is 40 m (Fig. 16). The resistivity profile is based on 2517 measurements by the terrameter. The measurements are presented as inverted 2D resistivity and IP-effect sections in Figs. 16 and 17, respectively. Fig. 17 has been limited to showing the maximum value 13mV/V, as it is the highest value seen outside the anomaly which shows much higher values. If the legend included the value of the anomaly present in the section, it would result in only two colours being shown in the section due to the very large contrast, making the IP-effect section very crude.

At the 25 m mark (Fig. 16) the profile crosses a small gravel track that runs along the length of the drumlin along its eastern side, which clearly comes out as an anomaly in both the resistivity and IP-effect sections. The IP-effect anomaly that can be seen at 25 m has a high value of ~70mV/V.

4.2.1.2 Interpretation

Based on the sections in Figs. 16 and 17, an interpreted model section has been constructed (Fig. 18). The anomaly at the 25 m mark has been interpreted as a measurement error, caused artificially. Potentially due to a cable or metal object under the gravel track. This is because the anomaly has very low resistivity of around 100Ωm and a chargeability of 70mV/V, which is a value approximately 7 times larger than any other IP-effect measured in this study. The shape seen in the inverted model is rectangular and strange looking. A substantial part of the interpreted model section is classified as 'indistinguishable' and can either be bedrock or sediment. The bedrock in profile 1 is undulating and the thickness and configuration of covering sediment seem to be independent from bedrock morphology.

4.2.1.3 Sediment depths

The sediment thickness along the profile is presented in Table 3, with interpreted maximum and minimum values. At the 110 m mark sediment thickness was

Table 4. The interpreted maximum and minimum thickness of sediment down to bedrock along profile 2. The (*) marks the sediment thickness at 70 m, which is the intersection with profile 5; at comparison between the two profiles the 3 m thickness is seen in both. The ([a]) marks indicate the presence of an anomaly .

Distance (m)	20[a]	30	50	70[a]	90	110	130
Max (m)	7		6	12	5	5	4
Min (m)	6	6	6	3*	4	5	2

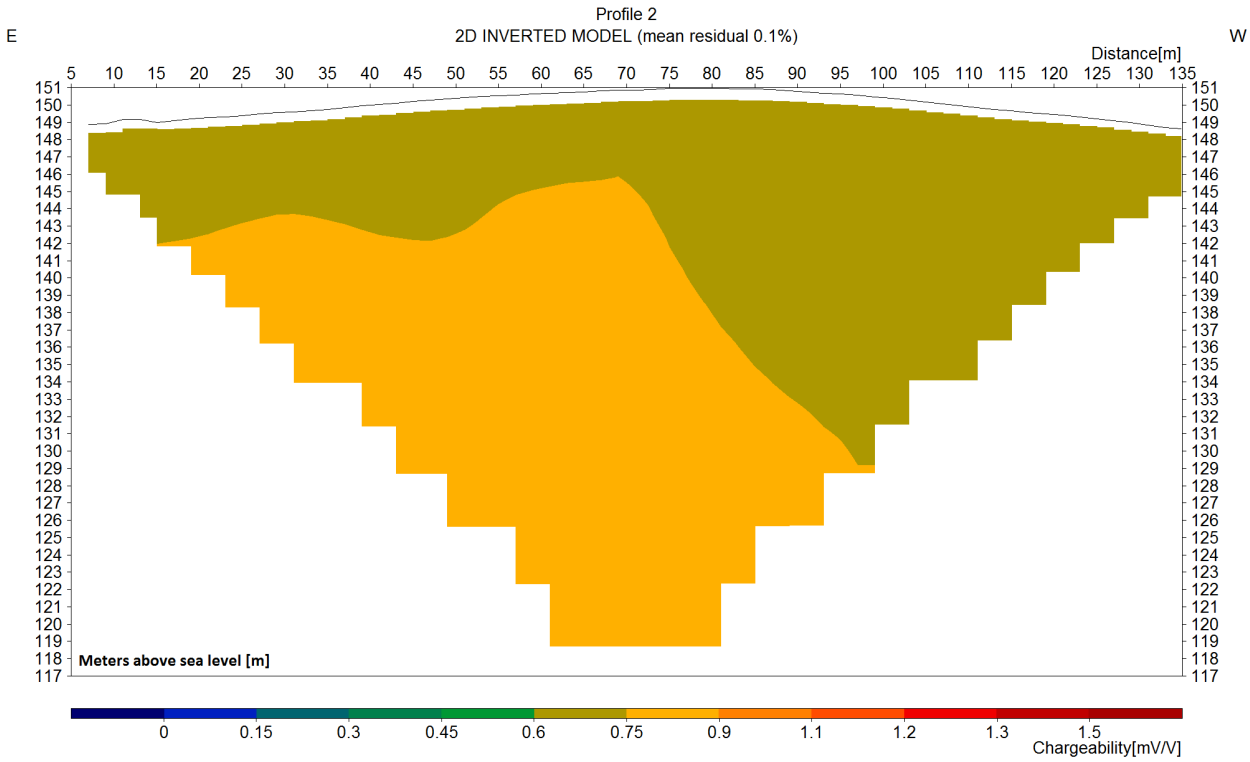

Fig 20. IP-effect section of profile 2.

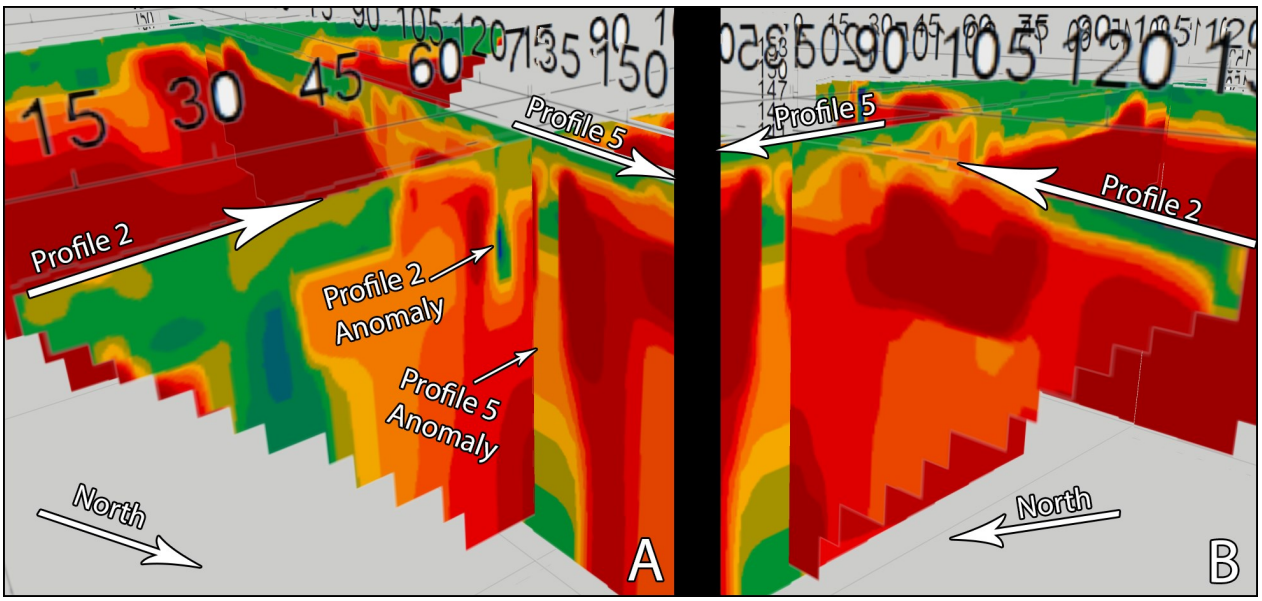

Fig 21. A) The intersection of the two resistivity sections of profiles 2 and 5, on the western side of the drumlin. The intersection is at the 75 m mark in profile 2. B) The east part of the resistivity section of profiles 2 and 5, from the 75 m to 135 m marks.

also measured in profile 5. Profile 5 does not indicate any 'indistinguishable' zone at this point and gives a sediment thickness here that is equal to the interpreted maximum thickness of profile 1, making this value more likely to be close to the true depth to bedrock.

4.2.2 Profile 2

4.2.2.1 Inverted models

Profile 2 (Fig. 13) measures 140 m in length, over which the maximum measurement depth is 34 m (Fig. 19). The resistivity profile is based on 1384 measurements by the terrameter. The measurements are presented as inverted 2D resistivity and IP-effect sections in Figs. 19 and 20, respectively.

At 18 m mark (Fig. 19) is the crossing with the drumlin-parallel gravel track, but no anomaly is seen as in profile 1. At approximately the 32 m and 70 m marks are vertically standing anomalies in the resistivity sec-

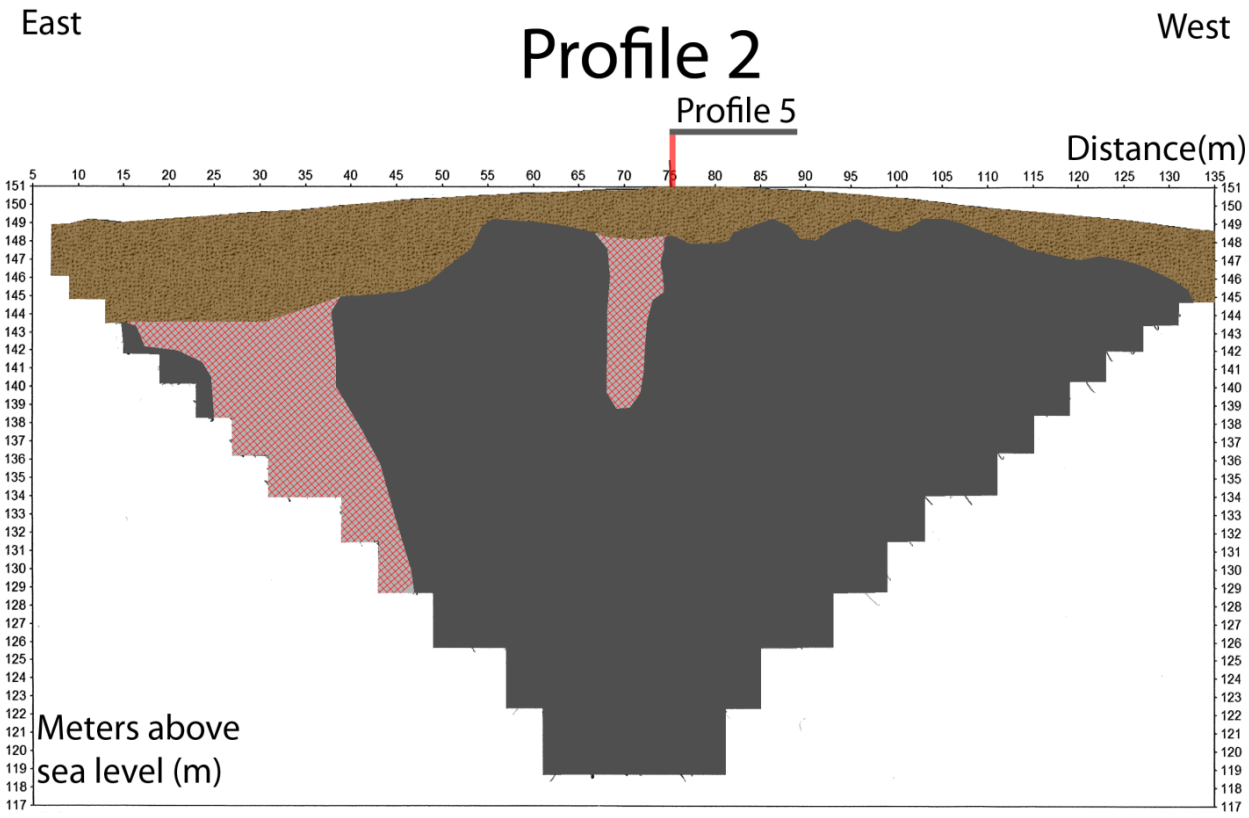

Fig 22. An interpreted geological model of profile 2. At 75 m a red line marks the crossing with profile 5. The unit marked as bedrock is very likely bedrock, and the unit marked as sediment very likely such, based on their high versus low resistivities, respectively (Table 1). The units marked indistinguishable and anomaly are zones where the bedrock and sediment could be

tion (Fig. 19). The IP-effect section gives very low values of around 0.7 mV/V throughout the profile.

4.2.2.2 Interpretation

Based on the sections in Figs. 19 and 20, an interpreted model section has been constructed (Fig. 22). The resistivity section shows two anomalies that cut through interpreted bedrock at the 32 and 70 m marks. The anomaly at 32 m shows values of around 200 to 300Ωm, but no anomaly in the IP-effect section. This indicates that the anomaly is not caused by disturbing objects in the ground with high IP-effect and that, if the anomaly is caused by weathered rock, then it does not contain clay. Profile 5 crosses profile 2 at the 75 m mark, which is close to the anomaly at 70 m. Profile 5 shows a deep anomaly close to where the two profiles intersect. Resolution decreases with depth and resistivity values are affected by its surroundings, also known as "3D-effects", as described in Jeppson & Dahlin (2015). The resistivity value in profile 1 is therefore affected by the nearby anomaly from profile 5, resulting in the small anomaly seen at 70 m (Fig. 21). The bedrock is undulating and the thickness and configuration of covering sediment seem to be independent of the bedrock morphology. The 'indistinguishable' zone in profile 2 is very small and has not been marked in the interpreted model in Fig. 22.

4.2.2.3 Sediment depths

The sediment thickness along the profile is presented in Table 4, with interpreted maximum and minimum values. The 70 m mark is close to the intersection with profile 5. The sediment thickness in profile 5 is here approximately 3 m. This is the same as the minimum thickness at 70 m in profile 2, making this a more likely value for the true sediment thickness.

Table 5. The interpreted maximum and minimum thickness of sediment down to the bedrock along profile 3.The ([a]) mark indi-

Distance (m)	15	35	45[a]	55	75	85
Max (m)	7	8		6	6	4
Min (m)	7	8	8	6	6	4

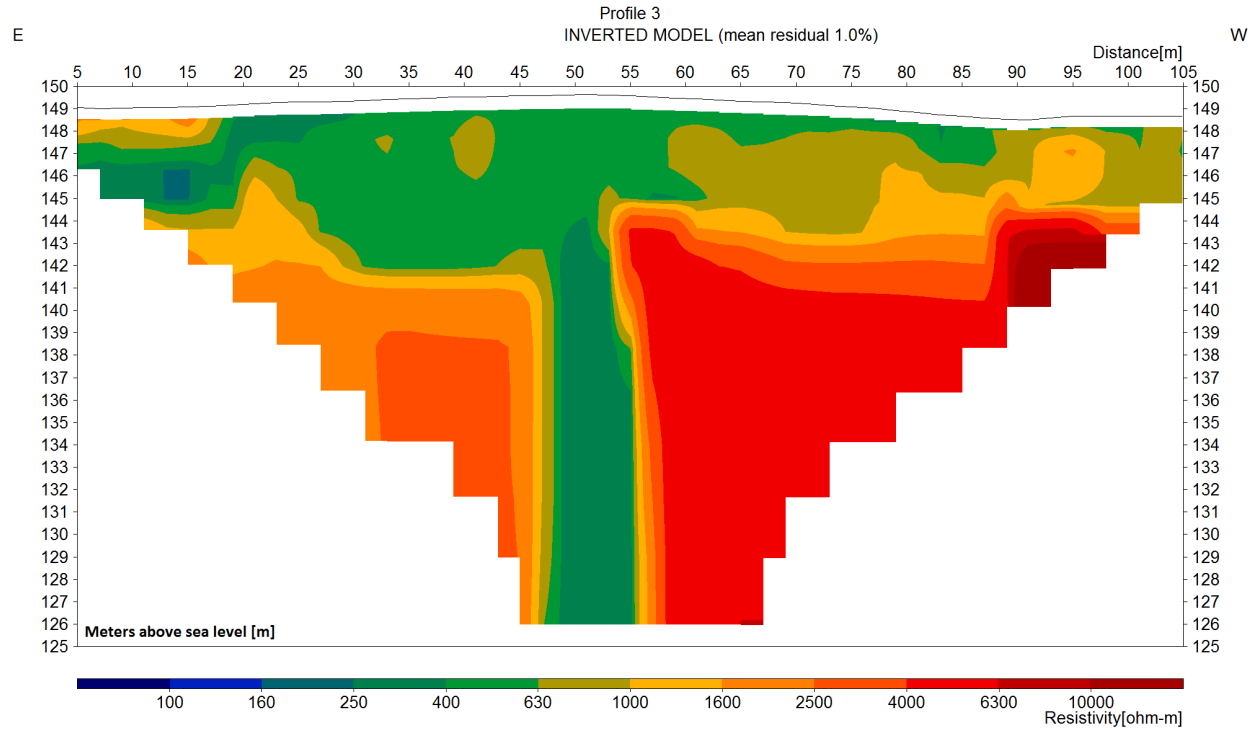

Fig 23. Resistivity section of profile 3.

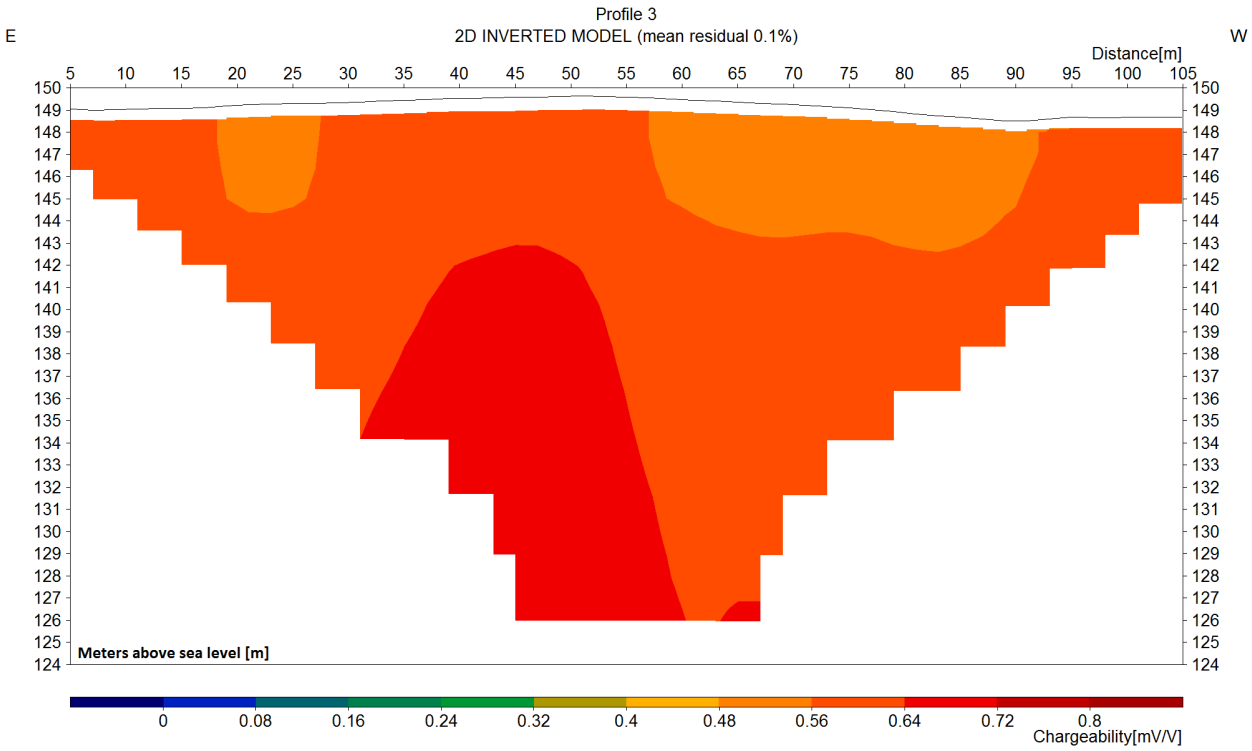

Fig 24. IP-effect section of profile 3.

4.2.3 Profile 3

4.2.3.1 Inverted models

Profile 3 (Fig. 13) measures 110 m in length, over which the maximum measurement depth is approximately 23 m. The resistivity profile is based on 863 measurements by the terrameter. The measurements are presented as inverted 2D resistivity and IP-effect sections in Figs. 23 and 24 respectively.

At the 15 m mark (Fig. 23) is the crossing with the drumlin-parallel gravel track, but no anomaly is seen as in profile 1. At approximately the 50 m mark is a vertically standing anomaly in the resistivity section

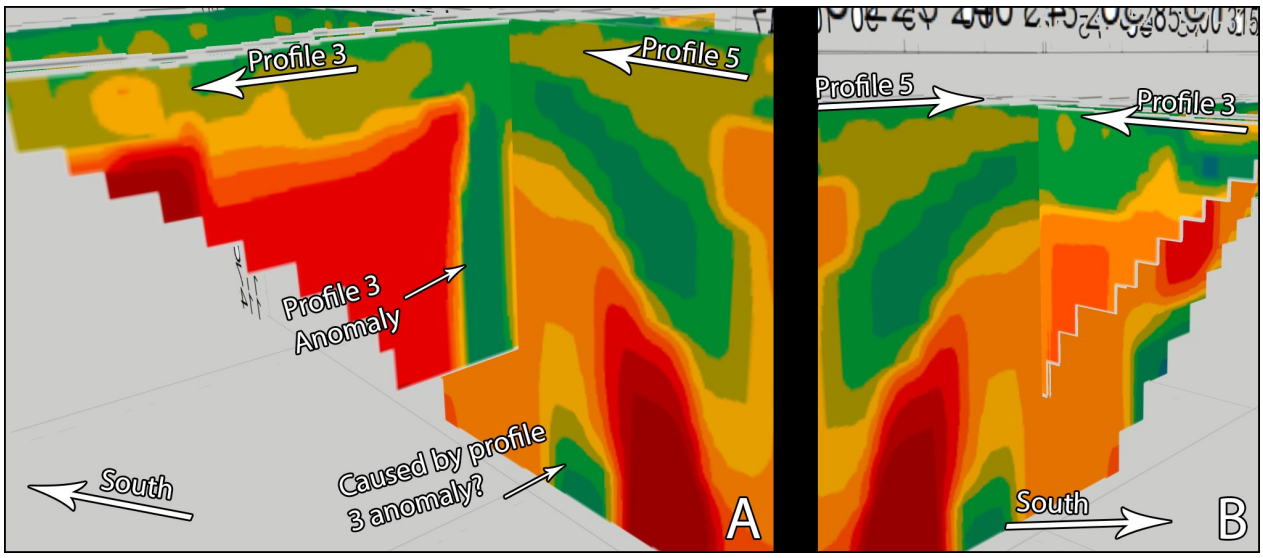

Fig 25. A) The intersection of the two resistivity sections profiles 2 and 5, on the western side of the drumlin. The intersection is

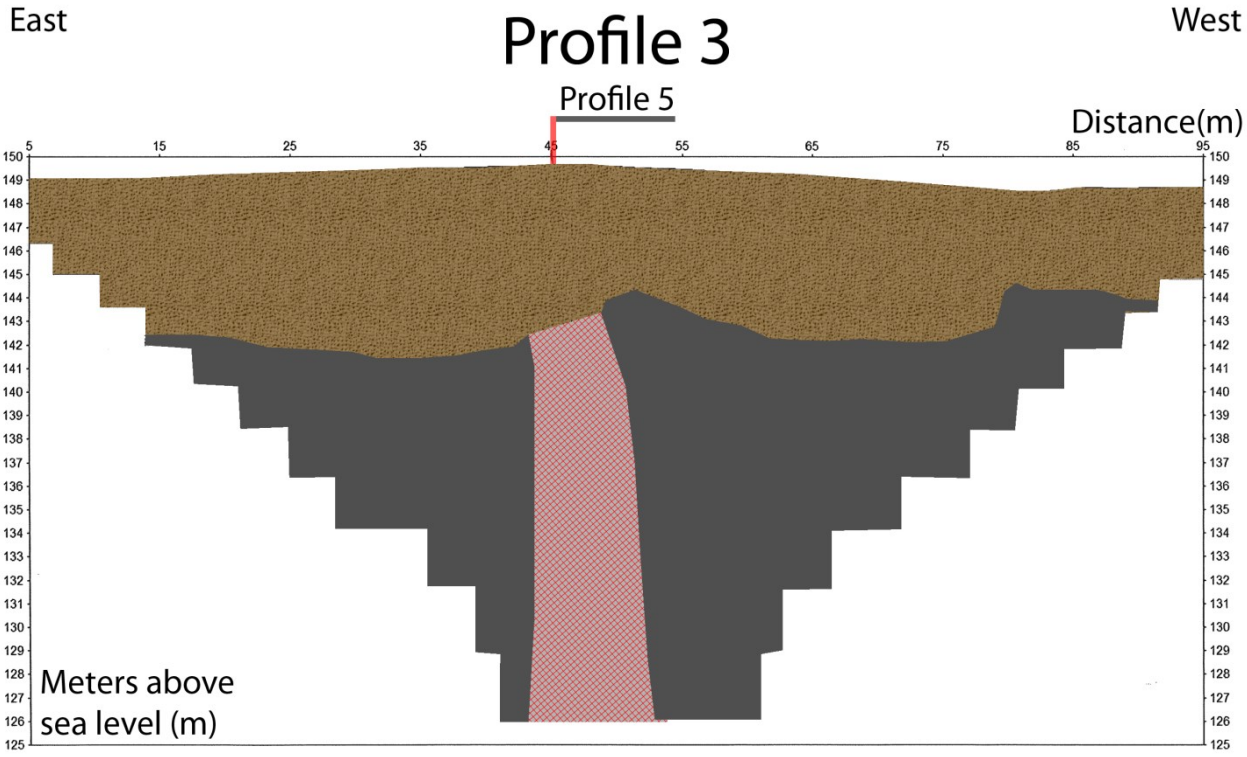

Fig 26. An interpreted geological model of profile 3. At 45 m a red line marks the crossing with profile 5. The unit marked as bedrock is very likely bedrock, and the unit marked as sediment is very likely such, based on their high versus low resistivities, respectively (Table 1).The units marked 'indistinguishable' and 'anomaly' are zones where the bedrock and sediment could be

(Fig 23). The IP-effect section gives very low values of around 0.6 mV/V throughout the section. (Fig. 24)

4.2.3.2 Interpretation

Based on the sections in Figs. 22 and 23, an interpreted model section has been constructed (Fig. 26). The resistivity section shows an anomaly that cut through the interpreted bedrock at the 48 ~m mark. The anomaly shows values of around 300Ωm, but only a difference in chargeability of approximately 0.1 mV/V to its surroundings. This indicates that the anomaly is not caused by disturbing objects with high IP-effect in the ground and that, if the anomaly is caused by weathered rock, then it does not contain clay. Profile 5 crosses profile 3 at the 45 m mark, which is close to the anomaly. The anomaly is not visible in profile 5 in the intersection, but at larger depths there are anomalies that could be connected to the anomaly from profile 3 (Fig.

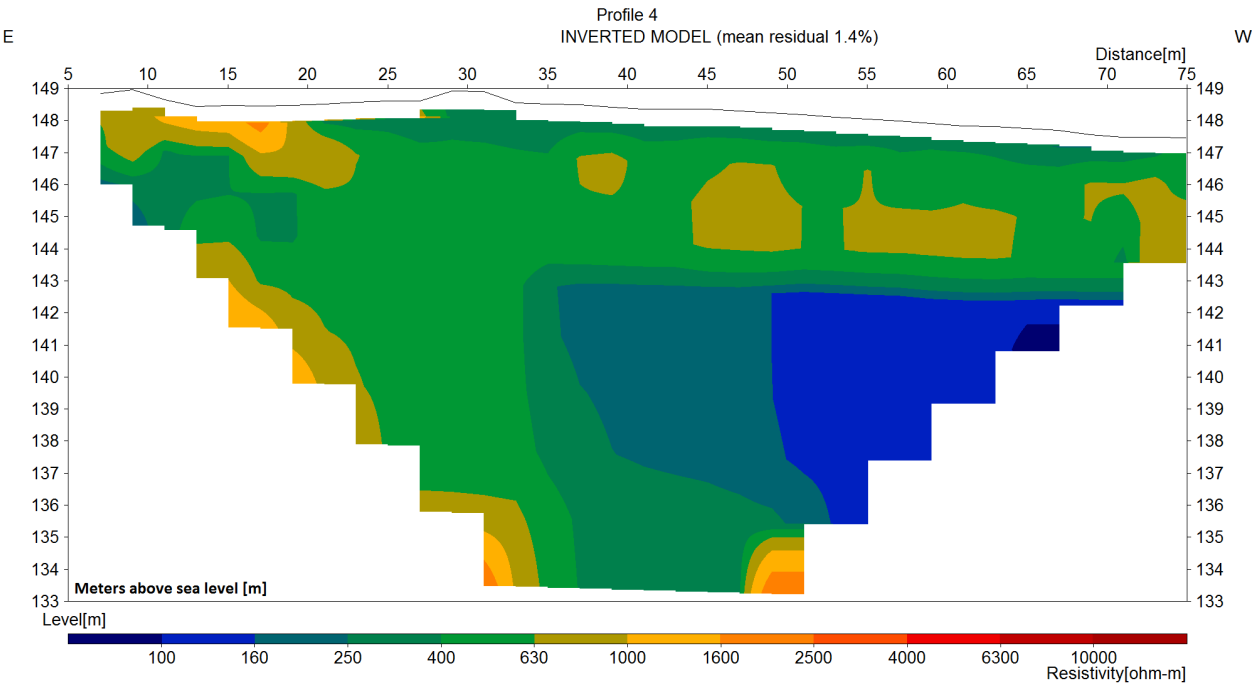

Fig 27. Resistivity section of profile 4.

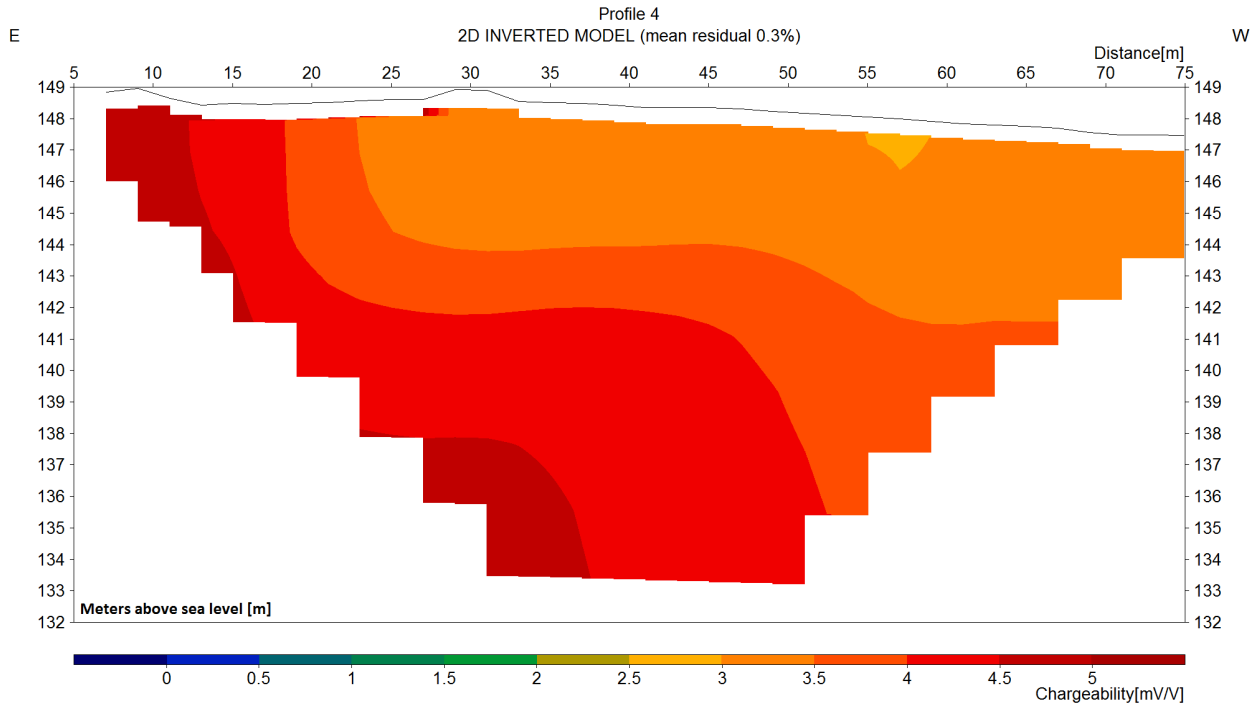

Fig 28. IP-effect section of profile 4.

25). The bedrock is undulating and the thickness and configuration of covering sediment seems to be independent of the bedrock morphology.

4.2.3.3 Sediment depths

The sediment thickness along the profile is presented in Table 5, with interpreted maximum and minimum values. The 45 m mark was also measured in profile 5 and gives a sediment thickness here of 9 m. The two profiles differ approximately 1 m in sediment thickness.

4.2.4 Profile 4

4.2.4.1 Inverted models

Profile 4 (Fig. 13) measures 80 m in length, over which the maximum measurement depth is approximately 16 m (Fig. 27). The resistivity profile is based on 486 measurements by the terrameter. The measure-

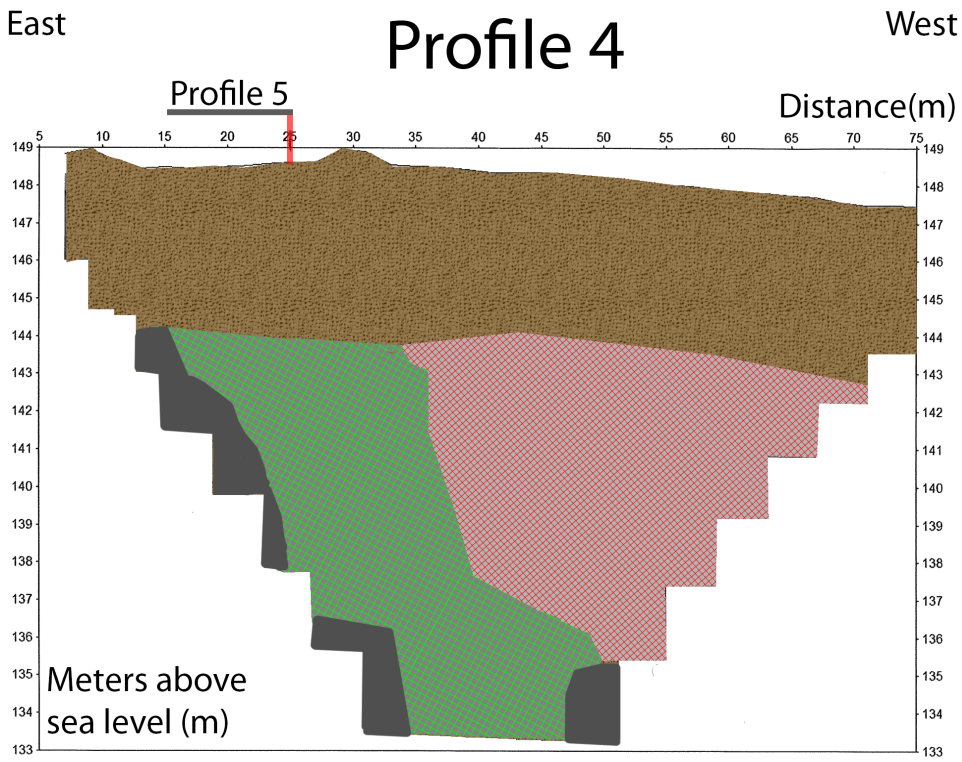

Fig 29. An interpreted geological model of profile 4. At 25 m a red line marks the crossing with profile 5. The unit marked as bedrock is very likely bedrock, and the unit marked as sediment very likely such, based on their high versus low resistivities respectively (Table 1). The units marked as 'indistinguishable' and as 'anomaly' are zones where the bedrock and sediment

ments are presented as inverted 2D resistivity and IP-effect sections in Figs. 27 and 28, respectively.

At the 16 m mark (Fig. 27) is the crossing with the drumlin-parallel gravel track, but no anomaly is seen as in profile 1. The entire resistivity section shows low values, ranging from 100 to 500 Ωm (Fig. 27). The IP-effect changes like a gradient from approximately 3.5 to 5mV/V throughout the section (Fig. 28).

4.2.4.2 *Interpretation*

Based on the sections in Figs. 27 and 28, an interpreted model section has been constructed (Fig. 28). The absence of resistivity values that interpret bedrock in the section does not have to mean there is no bedrock present. The resistivity section shows very low values of around 100 Ωm, from 35 to 70 m at 143 meters above sea level. It could be a more conductive type of

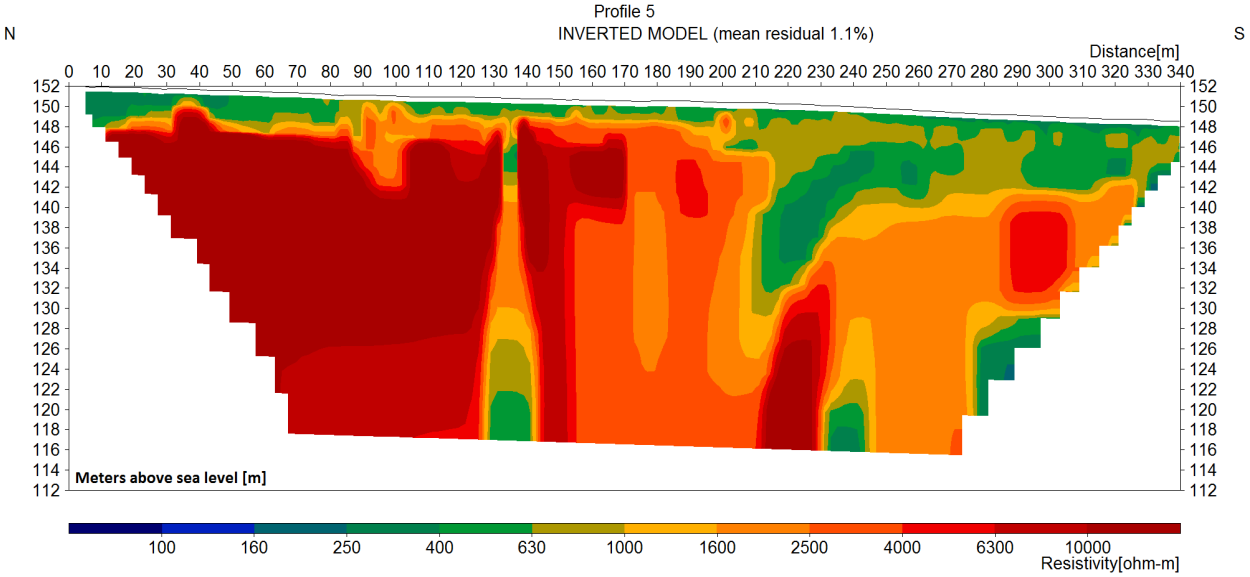

Fig 30. Resistivity section of profile 5.

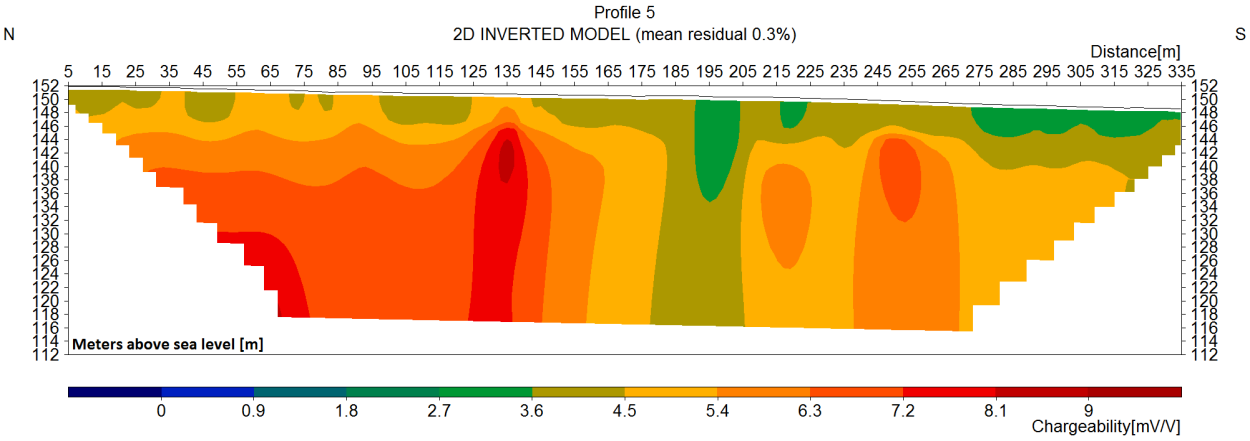

Fig 31. IP-effect section of profile 5.

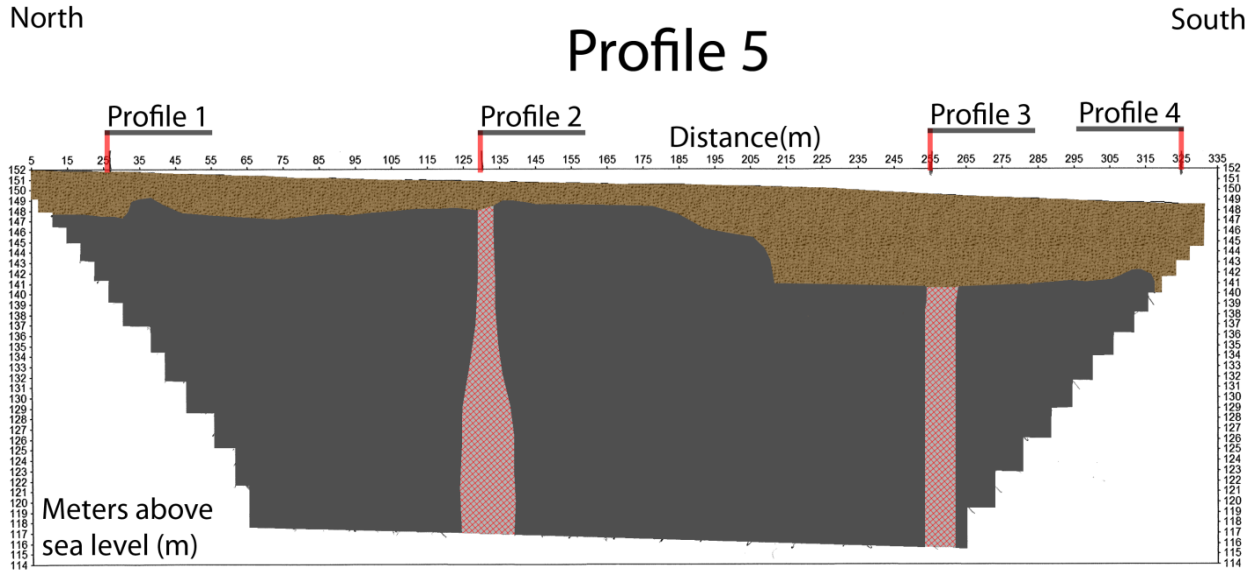

Fig 32. An interpreted geological model of profile 5. At 25, 130, 255 and 325 m the red lines mark where profiles 1, 2, 3 and 4 intersect with profile 5. The unit marked as bedrock is very likely bedrock, and the unit marked as sediment very likely such, based on their high versus low resistivities, respectively (Table 1). The units marked indistinguishable and anomaly are zones where the bedrock and sediment could be interpolated. Fig. 17 for the legend.

sediment or presence of water. A possibility is also that the sediment depth reaches to 143 m above sea level and the low resistivity values are due to fractures in rock. Profile 5 intersects with profile 4 at the 25 m mark and has a sediment thickness reaching approximately 143 m above sea level around this mark. There are no height-determined IP-values in that area. The profile length is short, and results in smaller investigation depths. This makes it harder to find the boundary between bedrock and soil. Profile 4 intersects in the end of Profile 5 which has low investigation depth at the intersection. Due to the complexity of the section, three different models are deemed possible:

1) The entire section consists of only sediment, as the resistivity values are very low.
2) The indistinguishable zone and the anomaly zone are both fractured rock.
3) The indistinguishable zone is either rock or sediment, and the anomaly zone is fractures in rock.

4.2.4.3 Sediment depths

In the intersection of profile 4 and 5 there are almost no resistivity values that confirm bedrock. Depending on which of the three models to use, the sediment

Table 6. The interpreted maximum and minimum thickness of sediment down to bedrock along profile. The (*) marks the sediment thickness at points that intersect and were also measured in another profile. The ([a]) mark indicates the presence of an

Distance (m)	25	85	130[a]	165	195	215	245	285	325
Max (m)	4*	4		2	4	9	9	8	6-15+*
Min (m)	4*	4	2*	2	4	9	9	8	5-7+*

thickness can vary with several meters. In model 1 the sediment thickness in profile 5 is at least 7+ meters in this area and profile 4 suggests at least 15+ meters. In model 2 and 3 of profile 4 the sediment thickness is approximately 5-6 m. Due to the low investigation

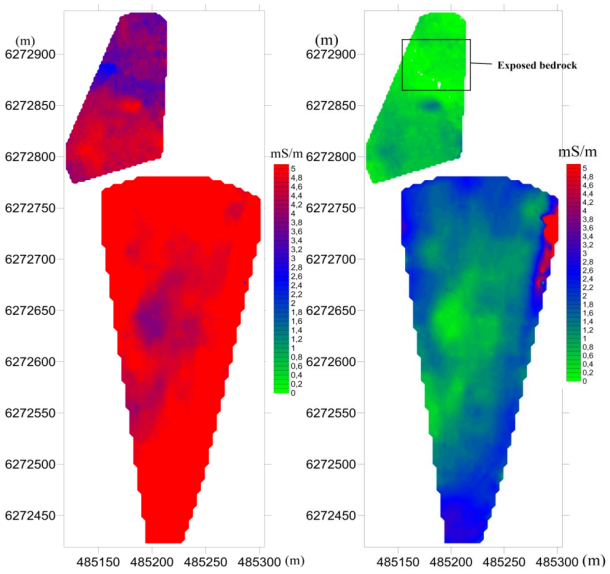

Fig 33.The apparent conductivity of the ground measured with slingram at the 35025 Hz (to the left) and 63375Hz (to the right) frequencies. The box in the centre image shows exposed bedrock. The image to the right shows the resistivity

depth and possible fractures in rock giving resulting in the low resistivity values that falsely give the impression of absence of bedrock, it is more likely that the sediment thickness is around 5-6m if compared to the thickness trend of the entire drumlin in the previous profile sections.

4.2.5 Profile 5

4.2.5.1 Inverted models

Profile 5 (Fig. 13) measures 346 m in length, over which the maximum measurement depth is 35 m. The resistivity profile is based on 5965 measurements by the terrameter. The measurements are presented as inverted 2D resistivity and IP-effect sections in Figs. 30 and 31, respectively.

At the approximately 135 m and 255 m marks, and at 120 meters above sea level, there are two dominant resistivity anomalies (Fig. 30). These two anomalies are also seen in the IP-effect section (Fig. 31) albeit clearer than in the resistivity section.

4.2.5.2 Interpretation

Based on the sections in Figs. 30 and 31, an interpreted model section has been constructed (Fig. 32). The resistivity section shows an anomaly that cut through the interpreted bedrock at the 135 and 255 m marks. The anomaly at the 135 m mark shows values of around 300 to 2000 Ωm and an anomaly in the IP-effect section. This anomaly is also weakly present in profile 2, but with a smaller thickness. This anomaly has been interpreted as fractures in rock. The width is approximately 2 meter, but shows a larger width at larger depth. This is likely due to lower resolution that comes with larger depths. The anomaly at the 255 m mark is also present in profile 3, and is clearly visible in the IP-effect section. Very low resistivities of around 400 Ωm is visible at 118 m above sea level at the 235 m and 285 m marks. These could be due to the fractures in rock, as suggested from profile 3 that is close by. Thus, the anomaly marked at 255 m is based on IP-data from profile 5 and resistivity data from profile 3 (Fig. 23). The bedrock has a sudden increase in sediment thickness at around 205 m. This interpreted increase in sediment thickness could be a misinterpretation, instead being fractured rock which could cause the lower resistivity values. The bedrock level was interpolated from 210 m to 240 m to be around 141 m above sea level due to the high resistivity values being interpreted as bedrock seen around this depth, at the 300 m mark (Fig. 30).

4.2.5.3 Sediment depths

The sediment thickness along the profile is presented in Table 6, with interpreted maximum and minimum values. The 25 m mark was also measured in profile 1. Profile 5 does not display any indistinguishable zone here; thus max/min thicknesses are the same. The 130 m mark was correlated with profile 2. The 325 m mark was discussed in the section regarding results from profile 4.

4.3 Electromagnetic slingram results

4.3.1 Conductivity data

The slingram measured with three different frequencies, albeit only the two higher frequencies gave usable data (Fig. 33). The lowest-frequency 18125 Hz did not give conductivity measurements that can be used for interpretation, since almost all conductivity data show values near 0 mS/m. The anomaly seen in the far right in Figs. 32 and 33 is due to disturbing objects such as vehicles and other metal objects. The X and Y axis use a grid system in UTM. The maximum value of the apparent conductivity in Figs. 32 and 33 were limited to 5 mS/m. However, the measurements at 35025 Hz and 63375 Hz gave interpretable data. The anomaly seen in the top right is also visible in profile 1 at the 25 m mark. Measurements at both frequencies show the same patterns, but with different values. There is a general trend of increase in conductivity from north to south. Another general trend is higher

conductivity values at the sides and lower values in the centre of the drumlin.

4.3.2 Interpretation

According to profile 1 in Table 3, the sediment thickness increases towards the centre of the profile and is lower at the sides. Yet the slingram measurements show a decrease in conductivity towards the centre of the profile according to Fig. 33. Considering that it is apparent conductivity, which is an average conductivity of the underlying ground, the values are not precise but rather relative. This could be interpreted as that the indistinguishable zone in profile 1 is more likely bedrock than sediment. In profile 2 the sediment thickness starts of at ~7 m in the east part of the profile and decreases towards the centre and the end of the profile. The slingram conductivity data conforms somewhat to this, with higher conductivity values in the beginning of the profile (Fig. 33), which is due to the higher sediment depth and the anomaly. The conductivity decreases in the centre of the profile where the sediment depth decreases. Profile 3, which show a sediment thickness of ~7 m in the east part of the profile has higher conductivity values throughout the profile according to the slingram data. The general increase of slingram conductivity from north to south conforms to the models presented in the interpreted resistivity section. According to profile 5 (Fig. 32) there is a large increase of approximately 5 m in soil depth at around the 210 m mark. Profile 4 also suggested large sediment thickness (Fig. 29), which is in line with the higher conductivity values in the south of the conductivity measurements (Fig. 33).

5 Discussion

As previously mentioned, the models presented suffer from what is mentioned in Jeppson & Dahlin (2015a) as an equivalence problem. This means that the resistivity sections could be interpreted in many different ways, and all being geologically sound. It should also be noted that the bedrock level is much approximated due to overlapping resistivity intervals between geological material and resolution, causing diffuse boundaries between different units. Due to the inaccuracy, the suggested sediment thicknesses should be considered indicators rather than exact values. The same applies for the electromagnetic slingram measurements that have no values to correlate certain depths to. These issues could be solved by drillings or excavations, because then certain resistivity values can be attributed to confirmed types of geological material. Due to equivalence problems, it is proposed that seismic refraction studies are might be a more suitable geophysical study compared to the three methods used in this study. Since the aim of this study is to find the sediment thicknesses in relation to bedrock, a refraction study is suggested to be tested as an alternative method since it could show a clearer contrast between bedrock and sediment, compared to performed resistivity measurements. This is because resistivity is affected in three dimensions and has to be inverted. However, if the sediment consists of different units/ types and with decreasing seismic speeds for occurring sediment type beds, then refraction studies might not be optimal. It is quite common that that the fracture zones in bedrock occur together with lithological changes. As mentioned in the section of geological background, there is a mapped change of bedrock type beneath the drumlin (Fig. 2). It is possible that the anomalies seen in the different profiles are caused by this lithological change. It was however not considered important to analyse the suspected fracture zones in more detail in this study more than noting that the displayed anomalies are due to fractures and not due to sediment changes

6 Conclusions

The sediment thickness on top of bedrock, as interpreted along four cross profiles and one longitudinal profile over the Rörvik gård drumlin varies between 2 – 8 m for calculated minimum values and between 2 – 15 m+ for calculated maximum values. The sediment thickness seems in general increase from the flanks of the drumlin towards its centreline and also increase towards the drumlin's tail. The bedrock surface beneath the drumlin has an undulating morphology and the smooth surface of the drumlins seems to be unrelated to that bedrock morphology. However, presented geophysical models are very crude and should only be taken as indicators of sediment thicknesses and not precise values as there are no drill logs or test pit information to calibrate the geophysical measurements with.

7 Acknowledgements

Gratitude is expressed to the fellow BSc student team that assisted with the field work, Jeanette Svendsen, Sofia Åkesson and Patrik Zaman, and to the supervisors Per Möller at Lund University and Hans Jeppsson at WSP that assisted and guided this study. Gratitude is also expressed to the Faculty of Engineering at Lund University and WSP for giving access to the geophysical instruments and equipment used in this study. Torleif Dahlin, Tom Dowling and others at the Department of Geology are thanked for the assistance provid-

ed. The farmer that helped with pulling out our minibus that was stuck in the mud is also thanked.

8 References

Barker, R., 1992: A simple algorithm for electrical imaging of the subsurface. First Break, 10, 2, 53-62

Hauck, C. & Kneisel, C., 2008: Applied Geophysics in Periglacial Environments. United States of America: Cambridge University Press. 240pp

Jeppson, H. & Dahlin, T., 2015a: Geoelektriska Metoder inom tillämpad geofysik, Resistivitetsmätning, IP-mätning, SP-mätning. Kompendium i Geofysiska undersökningsmetoder, GEOC04. Department of Geology,Lund University. 70pp

Jeppson, H. & Dahlin, T., 2015b: Elektromagnetiska Metoder. Kompendium i Geofysiska undersökningsmetoder, GEOC04. Department of Geology,Lund University. 122 pp

Lowrie, W., 2007: Fundementals of Geophysics. United States of America: Cambridge University Press. 381 pp

Milsom, J. & Eriksen, A., 2011: Field Geophysics. United Kingdom: John Wiley & Sons Ltd. 287 pp

Möller, P., 1987: Moraine morphology, till genesis, and deglaciation pattern in the Åsnen area, southwestern Småland, Sweden. *LUNDQUA Thesis 20*. Department of Geology, Lund University, Sweden, 146 pp.

Möller, P., 2010: Melt-out till and ribbed moraine formation, a case study from south Sweden. *Sedimentary Geology 232*, 161–180.

Möller, P. & Murray, A., accepted: Drumlinised glaciofluvial and glaciolacustrine sediments on the Småland peneplain, South Sweden – new evidence on the growth and decay history of the Fennoscandian Ice Sheets during MIS 3. *Quaternary Science Reviews x, xx-xx*. (DOI: 10.1016/j.quascirev.2015.04.025)

Möller, P., Dowling, T.P.F., accepted: The importance of thermal boundary transitions on glacial geomorphology; mapping of ribbed/hummocky moraine and streamlined terrain from LiDAR, over Småland, South Sweden. *GFF x*, xx-xx.

Reynolds, J.M., 1997: An Introduction to Applied and Environmental Geophysics. United Kingdom: John & Wiley & Sons Ltd. 796 pp

Wik, N-G., Claeson, D., Bergström, U., Hellström, F., Jelinek, C., Juhojuntti, N., Jönberger, J., Kero, L., Lundqvist, L., Sukotjo, S & Wikman, H., 2009: Beskrivning till regional berggrundskarta över Kronobergs län. Sveriges Geologiska Undersökning K 142. Sweden: Tabergs Tryckeri AB. 68 pp

Zaman, P., 2015: LIDAR mapping of presumed rock-cored drumlins in the Lake Åsnen area, Småland, South Sweden. Department of Geology, Lund University. 13 pp

Zohdy, A.A.R, 1989: A new method for the automatic interpretation of Schlumberger and Wenner sounding curves. Geophysics, 54 (2), 245-253.

Internet sources

Image and Appendix sources

SGU Bedrock map: http://apps.sgu.se/kartvisare/kartvisare-berggrund-1-miljon-sv.html - 150512

Location of Småland in Sweden: http://sv.wikipedia.org/wiki/Sm%C3%A5land#/media/File:Sverigekarta-Landskap_Sm%C3%A5land.svg – 150512

Map of the drumlin area: http://kso2.lantmateriet.se/ - 150512

Location of profiles on drumlin: https://www.google.se/maps/@56.5977181,14.7592403,633m/data=!3m1!1e3 – 150512

9 Appendix

Inversion settings

Initial damping factor (0.01 to 1.00)
0.1500
Minimum damping factor (0.001 to 0.75)
0.0200
Local optimization option (0=No, 1=Yes)
0
Convergence limit for relative change in RMS error in percent (0.1 to 20)
5.0000
Minimum change in RMS error for line search in percent (0.5 to 100)
0.5000
Number of iterations (1 to 30)
7
Vertical to horizontal flatness filter ratio (0.25 to 4.0)
1.0000
Model for increase in thickness of layers(0=default 10%, 1=default 25%, 2=user defined)
2
Number of nodes between adjacent electrodes (2 or 4)
4
Flatness filter type, Include smoothing of model resistivity (0=model changes only,1=directly on model)
1
Reduce number of topographical data points? (0=No,1=Yes. Recommend leave at 0)
0
Carry out topography modeling? (0=No,1=Yes)
1
Type of topography trend removal (0=Average,1=Least-squares,2=End to end)
2
Type of Jacobian matrix calculation (0=Quasi-Newton, 1=Gauss-Newton, 2=Mixed)
1
Increase of damping factor with depth (1.0 to 2.0)
1.0500
Type of topographical modeling (0=None, 1=No longer supported so do not use, 2=uniform distorted FEM, 3=underwater, 4=damped FEM, 5=FEM with inverse Swartz-Christoffel)
4
Robust data constrain? (0=No, 1=Yes)
1
Cutoff factor for data constrain (0.0001 to 0.1))
0.0500
Robust model constrain? (0=No, 1=Yes)
1
Cutoff factor for model constrain (0.0001 to 1.0)
0.0050
Allow number of model parameters to exceed data points? (0=No, 1=Yes)
1
Use extended model? (0=No, 1=Yes)
0
Reduce effect of side blocks? (0=No, 1=Slight, 2=Severe, 3=Very Severe)
1
Type of mesh (0=Normal,1=Fine,2=Finest)
0
Optimise damping factor? (0=No, 1=Yes)
1
Time-lapse inversion constrain (0=None,1&2=Smooth,3=Robust)
3
Type of time-lapse inversion method (0=Simultaneous,1=Sequential)
0
Thickness of first layer (0.25 to 1.0)
0.5000
Factor to increase thickness layer with depth (1.0 to 1.25)
1.1000
USE FINITE ELEMENT METHOD (YES=1,NO=0)
1
WIDTH OF BLOCKS (1=NORMAL WIDTH, 2=DOUBLE, 3=TRIPLE, 4=QUADRAPLE, 5=QUINTIPLE)
1
MAKE SURE BLOCKS HAVE THE SAME WIDTH (YES=1,NO=0)
1
RMS CONVERGENCE LIMIT (IN PERCENT)
0.100
USE LOGARITHM OF APPARENT RESISTIVITY (0=USE LOG OF APPARENT RESISTIVITY, 1=USE RESISTANCE VALUES, 2=USE APPARENT RESISTIVITY)
0
TYPE OF IP INVERSION METHOD (0=CONCURRENT,1=SEQUENTIAL)
0
PROCEED AUTOMATICALLY FOR SEQUENTIAL METHOD (1=YES,0=NO)
0
IP DAMPING FACTOR (0.01 to 1.0)
1.000
USE AUTOMATIC IP DAMPING FACTOR (YES=1,NO=0)
0
CUTOFF FACTOR FOR BOREHOLE DATA (0.0005 to 0.02)
0.00010
TYPE OF CROSS-BOREHOLE MODEL (0=normal,1=halfsize)
0
LIMIT RESISTIVITY VALUES(0=No,1=Yes)
0
Upper limit factor (10-50)
50.000
Lower limit factor (0.02 to 0.1)
0.020
Type of reference resistivity (0=average,1=first iteration)
0

Model refinement (1.0=Normal,0.5=Half-width cells)
1.00
Combined Combined Marquardt and Occam inversion (0=Not used,1=used)
0
Type of optimisation method (0=Gauss-Newton,2=Incomplete GN)
2
Convergence limit for Incomplete Gauss-Newton method (0.005 to 0.05)
0.005
Use data compression with Incomplete Gauss-Newton (0=No,1=Yes)
0
Use reference model in inversion (0=No,1=Yes)
1
Damping factor for reference model (0.0 to 0.3)
0.01000
Use fast method to calculate Jacobian matrix. (0=No,1=Yes)
1
Use higher damping for first layer? (0=No,1=Yes)
1
Extra damping factor for first layer (1.0 to 100.0)
5.00000
Type of finite-element method (0=Triangular,1=Trapezoidal elements)
1
Factor to increase model depth range (1.0 to 5.0)
1.050
Reduce model variations near borehole (0=No, 1=Yes)
0
Factor to control the degree variations near the boreholes are reduced (2 to 100)
5.0
Factor to control variation of borehole damping factor with distance (0.5 to 5.0)
1.0
Floating electrodes survey inversion method (0=use fixed water layer, 1=Incorporate water layer into the model)
1
Resistivity variation within water layer (0=allow resistivity to vary freely,1=minimise variation)
1
Use sparse inversion method for very long survey lines (0=No, 1=Yes)
0
Optimize Jacobian matrix calculation (0=No, 1=Yes)
0
Automatically switch electrodes for negative geometric factor (0=No, 1=Yes)
1
Force resistance value to be consistant with the geometric factor (0=No, 1=Yes)
0
Shift the electrodes to round up positions of electrodes (0=No, 1=Yes)
0
Use difference of measurements in time-lapse inversion (0=No,1=Yes)
0
Use active constraint balancing (0=No,1=Yes)
0
Type of active constraints (0=Normal,1=Reverse)
0
Lower damping factor limit for active constraints
0.4000
Upper damping factor limit for active constraints
2.5000
Water resistivity variation damping factor
8.0000
Use automatic calculation for change of damping factor with depth (0=No,1=Yes)
0

Tidigare skrifter i serien ”Examensarbeten i Geologi vid Lunds universitet”:

395. Rooth, Richard, 2014: Uppföljning av utlastningsgrad vid Dannemora gruva; april 2012 - april 2014. (15 hp)
396. Persson, Daniel, 2014: Miljögeologisk undersökning av deponin vid Getabjär, Sölvesborg. (15 hp)
397. Jennerheim, Jessica, 2014: Undersökning av långsiktiga effekter på mark och grundvatten vid infiltration av lakvatten – fältundersökning och utvärdering av förhållanden vid Kejsarkullens avfallsanläggning, Hultsfred. (15 hp)
398. Särman, Kim, 2014: Utvärdering av befintliga vattenskyddsområden i Sverige. (15 hp)
399. Tuvesson, Henrik, 2014: Från hav till land – en beskrivning av geologin i Skrylle. (15 hp)
400. Nilsson Brunlid, Anette, 2014: Paleoekologisk och kemisk-fysikalisk undersökning av ett avvikande sedimentlager i Barsebäcks mosse, sydvästra Skåne, bil dat för ca 13 000 år sedan. (15 hp)
401. Falkenhaug, Jorunn, 2014: Vattnets kretslopp i området vid Lilla Klåveröd: ett kunskapsprojekt med vatten i fokus. (15 hp)
402. Heingård, Miriam, 2014: Long bone and vertebral microanatomy and osteohistology of ’Platecarpus’ ptychodon (Reptilia, Mosasauridae) – implications for marine adaptations. (15 hp)
403. Kall, Christoffer, 2014: Microscopic echinoderm remains from the Darriwilian (Middle Ordovician) of Västergötland, Sweden – faunal composition and applicability as environmental proxies. (15 hp)
404. Preis Bergdahl, Daniel, 2014: Geoenergi för växthusjordbruk – Möjlig anläggning av värme och kyla i Västskåne. (15 hp)
405. Jakobsson, Mikael, 2014: Geophysical characterization and petrographic analysis of cap and reservoir rocks within the Lund Sandstone in Kyrkheddinge. (15 hp)
406. Björnfors, Oliver, 2014: A comparison of size fractions in faunal assemblages of deep-water benthic foraminifera—A case study from the coast of SW-Africa.. (15 hp)
407. Rådman, Johan, 2014: U-Pb baddeleyite geochronology and geochemistry of the White Mfolozi Dyke Swarm: unravelling the complexities of 2.70-2.66 Ga dyke swarms on the eastern Kaapvaal Craton, South Africa. (45 hp)
408. Andersson, Monica, 2014: Drumliner vid moderna glaciärer — hur vanliga är de? (15 hp)
409. Olsenius, Björn, 2014: Vinderosion, sanddrift och markanvändning på Kristianstadsslätten. (15 hp)
410. Bokhari Friberg, Yasmin, 2014: Oxygen isotopes in corals and their use as proxies for El Niño. (15 hp)
411. Fullerton, Wayne, 2014: REE mineralisation and metasomatic alteration in the Olserum metasediments. (45 hp)
412. Mekhaldi, Florian, 2014: The cosmic-ray events around AD 775 and AD 993 - Assessing their causes and possible effects on climate. (45 hp)
413. Timms Eliasson, Isabelle, 2014: Is it possible to reconstruct local presence of pine on bogs during the Holocene based on pollen data? A study based on surface and stratigraphical samples from three bogs in southern Sweden. (45 hp)
414. Hjulström, Joakim, 2014: Bortforsling av kaxblandat vatten från borrningar via dagvattenledningar: Riskanalys, karaktärisering av kaxvatten och reningsmetoder. (45 hp)
415. Fredrich, Birgit, 2014: Metadolerites as quantitative P-T markers for Sveconorwegian metamorphism, SW Sweden. (45 hp)
416. Alebouyeh Semami, Farnaz, 2014: U-Pb geochronology of the Tsineng dyke swarm and paleomagnetism of the Hartley Basalt, South Africa – evidence for two separate magmatic events at 1.93-1.92 and 1.88-1.84 Ga in the Kalahari craton. (45 hp)
417. Reiche, Sophie, 2014: Ascertaining the lithological boundaries of the Yoldia Sea of the Baltic Sea – a geochemical approach. (45 hp)
418. Mroczek, Robert, 2014: Microscopic shock-metamorphic features in crystalline bedrock: A comparison between shocked and unshocked granite from the Siljan impact structure. (15 hp)
419. Balija, Fisnik, 2014: Radon ett samhällsproblem - En litteraturstudie om geologiskt sammanhang, hälsoeffekter och möjliga lösningar. (15 hp)
420. Andersson, Sandra, 2014: Undersökning

av kalciumkarbonatförekomsten i infiltrationsområdet i Sydvattens vattenverk, Vombverket. (15 hp)

421. Martin, Ellinor, 2014: Chrome spinel grains from the Komstad Limestone Formation, Killeröd, southern Sweden: A high-resolution study of an increased meteorite flux in the Middle Ordovician. (45 hp)
422. Gabrielsson, Johan, 2014: A study over Mg/Ca in benthic foraminifera sampled across a large salinity gradient. (45 hp)
423. Ingvaldson, Ola, 2015: Ansvarsutredningar av tre potentiellt förorenade fastigheter i Helsingborgs stad. (15 hp)
424. Robygd, Joakim, 2015: Geochemical and palaeomagnetic characteristics of a Swedish Holocene sediment sequence from Lake Storsjön, Jämtland. (45 hp)
425. Larsson, Måns, 2015: Geofysiska undersökningsmetoder för geoenergisystem. (15 hp)
426. Hertzman, Hanna, 2015: Pharmaceuticals in groundwater - a literature review. (15 hp)
427. Thulin Olander, Henric, 2015: A contribution to the knowledge of Fårö's hydrogeology. (45 hp)
428. Peterffy, Olof, 2015: Sedimentology and carbon isotope stratigraphy of Lower–Middle Ordovician successions of Slemmestad (Oslo-Asker, Norway) and Brunflo (Jämtland, Sweden). (45 hp)
429. Sjunnesson, Alexandra, 2015: Spårämnesförsök med nitrat för bedömning av spridning och uppehållstid vid återinfiltrationav grundvatten. (15 hp)
430. Henao, Victor, 2015: A palaeoenvironmental study of a peat sequence from Iles Kerguelen (49° S, Indian Ocean) for the Last Deglaciation based on pollen analysis. (45 hp)
431. Landgren, Susanne, 2015: Using calcein-filled osmotic pumps to study the calcification response of benthic foraminifera to induced hypoxia under *in situ* conditions: An experimental approach. (45 hp)
432. von Knorring, Robert, 2015: Undersökning av karstvittring inom Kristianstadsslättens NV randområde och bedömning av dess betydelse för grundvattnets sårbarhet. (30 hp)
433. Rezvani, Azadeh, 2015: Spectral Time Domain Induced Polarization - Factors Affecting Spectral Data Information Content and Applicability to Geological Characterization. (45 hp)
434. Vasilica, Alexander, 2015: Geofysisk karaktärisering av de ordoviciska kalkstensenheterna på södra Gotland. (15 hp)
435. Olsson, Sofia, 2015: Naturlig nedbrytning av klorerade lösningsmedel: en modellering i Biochlor baserat på en fallstudie. (15 hp)
436. Huitema, Moa, 2015: Inventering av föroreningar vid en brandövningsplats i Linköpings kommun. (15 hp)
437. Nordlander, Lina, 2015: Borrningsteknikens påverkan vid provtagning inför dimensionering av formationsfilter. (15 hp)
438. Fennvik, Erik, 2015: Resistivitet och IP-mätningar vid Äspö Hard Rock Laboratory. (15 hp)
439. Pettersson, Johan, 2015: Paleoekologisk undersökning av Triberga mosse, sydöstra Öland. (15 hp)
440. Larsson, Alfred, 2015: Mantelplymer - realitet eller *ad hoc*? (15 hp)
441. Holm, Julia, 2015: Markskador inom skogsbruket - jordartens betydelse (15 hp)
442. Åkesson, Sofia, 2015: The application of resistivity and IP-measurements as investigation tools at contaminated sites - A case study from Kv Renen 13, Varberg, SW Sweden. (45 hp)
443. Lönsjö, Emma, 2015: Utbredningen av PFOS i Sverige och världen med fokus på grundvattnet – en litteraturstudie. (15 hp)
444. Asani, Besnik, 2015: A geophysical study of a drumlin in the Åsnen area, Småland, south Sweden. (15 hp)

LUNDS UNIVERSITET

Geologiska institutionen
Lunds universitet
Sölvegatan 12, 223 62 Lund